Matrix elements relevant for $\Delta I=1/2$ rule and ε'/ε from lattice QCD with staggered fermions

D. Pekurovsky* and G. Kilcup
Department of Physics, The Ohio State University, 174 West 18th Avenue, Columbus, Ohio 43210
(Received 19 May 1999; revised manuscript received 25 May 2001; published 4 September 2001)

We perform a study of matrix elements relevant for the $\Delta I=1/2$ rule and the direct CP violation parameter ε'/ε from first principles by computer simulation in lattice QCD. We use staggered (Kogut-Susskind) fermions, and employ chiral perturbation theory to study $K^0\to\pi\pi$ decays. Having obtained a reasonable statistical accuracy, we observe an enhancement of the $\Delta I=1/2$ amplitude, consistent with experiment within our large systematic errors. Finite volume and quenching effects have been studied and were found small compared to noise. The estimates of ε'/ε are hindered by large uncertainties associated with operator matching. In this paper we explain the simulation method, present the results and address the systematic uncertainties.

DOI: 10.1103/PhysRevD.64.074502 PACS number(s): 12.38.Gc, 11.15.Ha, 11.30.Er, 13.25.Es

I. INTRODUCTION

In those areas of particle phenomenology which require addressing nonperturbative effects, lattice gauge theory plays an increasingly significant role, being a first-principles method. The rapid advances in computational performance as well as algorithmic techniques are allowing us to apply lattice gauge theory to a wider range of problems than ever before.

In this paper we address the phenomenology of $K^0\to\pi\pi$ decays. Our goal is to compute $\langle\pi\pi|O_i|K^0\rangle$ matrix elements for all four-fermion operators in the basis of the $\Delta S=1$ effective weak Hamiltonian (introduced in Sec. II A).

We had several physical quantities in mind when doing our calculations. One is contained in the "$\Delta I=1/2$ rule," which is the observation that the transition channel of $K\to\pi\pi$ decays with isospin changing by 1/2 is enhanced 22 times with respect to transitions with isospin changing by 3/2. This is a well-known, long-standing puzzle in kaon phenomenology. Strong interactions are essential for explaining this effect within the standard model. Since the energy scales involved in these decays are rather small, computations in quantum chromodynamics (QCD) have to be done using a nonperturbative method such as lattice QCD. In particular, lattice QCD is used to calculate the hadronic matrix elements of the operators appearing in the $\Delta S=1$ effective weak Hamiltonian. Confirming the agreement of theory and experiment with regard to this phenomenon would be very important.

In addition, we address the related issue of ε', the direct CP-violation parameter in the neutral kaon system. There is now compelling experimental evidence that this parameter is nonzero. The Fermilab KTeV group's [1] most recent result is $\mathrm{Re}(\varepsilon'/\varepsilon)=(28.0\pm4.1)\times10^{-4}$, while the CERN NA48 group [2] reports $\mathrm{Re}(\varepsilon'/\varepsilon)=(18.5\pm7.3)\times10^{-4}$. Results from a third independent experiment at Frascati are expected soon. The world average based on both old and new results is currently $(19.3\pm3.6)\times10^{-4}$, more than 5σ above zero. On the theoretical side, the progress in estimating ε'/ε in the standard model has to rely on nonperturbative techniques of computing matrix elements of the appropriate basis operators [3], in this case using lattice QCD, and this is another purpose of our work.

We will introduce the methods employed in this work in detail in appropriate sections. Here we would like to say a few general words about them.

We employ the method of chiral perturbation theory, using it in its lowest order to combine our numerical results for $\langle\pi^+|O_i|K^+\rangle$ and $\langle0|O_i|K^0\rangle$ matrix elements to obtain $\langle\pi\pi|O_i|K^0\rangle$. Compared to the previous attempt [4] to compute them on the lattice with staggered fermions, this work introduces a number of improvements. The matrix elements are computed using ensembles with two different lattice spacings ($\beta=6.0$ and $\beta=6.2$ quenched ensembles). We have a significant increase in statistics (70 times for $\beta=6.0$, coming from both an increased number of configurations and number of noise samples per configuration). As a result of this increase the statistical accuracy of our results for both $\Delta I=1/2$ and $\Delta I=3/2$ amplitudes, $\langle\pi\pi|O_6|K^0\rangle$, $\langle\pi\pi|O_8|K^0\rangle$ and other matrix elements is finally under control. In this work we also consider operator matching, while in the previous work this issue was ignored. And finally, we study quenching effects by considering an $N_f=2$ ensemble at $\beta=5.7$.

Several other attempts to study the matrix elements in question have been reported from various lattice groups using either staggered or Wilson fermions (Refs. [5–9], reviews in Refs. [7,10]), but they fell short of desired accuracy because of technical difficulties and/or insufficient statistics. In addition, several groups [11,6,9] have studied matrix elements $\langle\pi^+\pi^0|O_i|K^+\rangle$ with good accuracy. However, these matrix elements describe only $\Delta I=3/2$, not $\Delta I=1/2$ transition, and so are not enough to study either the $\Delta I=1/2$ rule or ε'/ε.

Most recently, several attempts to compute the matrix elements in question using domain wall fermions have been initiated (Refs. [12–15]). This is a promising technique which has certain advantages and disadvantages compared to staggered fermions. On the one hand, domain wall fermions afford, in principle, the presence of full chiral symmetry at final cutoff without the complications due to an additional

*Current address: MC 0505, San Diego Supercomputing Center, 9500 Gilman Drive, La Jolla, CA 92093.

flavor of fermions as in the staggered fermions case. The chiral symmetry, however, requires a price to be paid in terms of added (fifth) dimension of the lattice which significantly increases the computational load. Therefore in practice one uses final N_5 (or L_s), which translates into residual chiral symmetry breaking effects and can have a high impact on calculating certain quantities. In particular, calculation of matrix elements considered in this work is subject to significant complications since they depend on gross cancellation between their components and hence are very sensitive to chiral symmetry. These problems are discussed in detail in Ref. [15]. Therefore it remains to be shown whether domain wall fermions indeed offer an advantage in the practical matter of computing $\langle \pi^+ \pi^0 | O_i | K^+ \rangle$ matrix elements.

Our calculations confirm significant enhancement of the $\Delta I = 1/2$ channel, consistent with the experimental value within the estimated uncertainty. Unfortunately the latter uncertainty is significant. Even though the statistical accuracy is very reasonable, there is another significant source of error in these complicated calculations, namely the uncertainties due to ignoring higher orders in chiral expansion, which also contain final state interactions. This error is common to any method using chiral perturbation theory, which includes most work in this area at present.

Another significant source of uncertainty, which influences mostly ε'/ε, but not $\Delta I = 1/2$ results, is due to perturbative operator matching, or the partially nonperturbative operator renormalization procedure, which we implement as a temporary step in cases where lattice perturbation theory breaks down. This uncertainty is the main obstacle to getting a reliable estimate of ε'/ε.

Speaking of the central value, we are seeing the negative sign of $\mathrm{Re}(\varepsilon'/\varepsilon)$, whereas the experiment shows it to be positive. Since systematic uncertainties entering our work are admittedly very large, it is too soon to call the standard model dead based on this result. However, it is still an interesting finding, and we are eager to see if other lattice groups confirm it.

The paper is structured as follows. In Sec. II we show the context of our calculations, define the quantities we are looking after, and discuss a number of theoretical points relevant for the calculation. Section III discusses issues pertaining to lattice simulations. In Sec. IV we present the results and discuss systematic errors for $\Delta I = 1/2$ rule amplitudes. In Sec. V we explain how the operator matching problem together with other systematic errors preclude a reliable calculation of ε'/ε, and give our best estimates for this quantity in Sec. VI. Section VII contains the conclusion. In the Appendices we give details about the quark operators and sources, and provide explicit expressions for all contractions and matrix elements. We also list our raw lattice results for all contractions involved.

II. THEORETICAL FRAMEWORK

A. Framework and definitions

The standard approach in applying theory to topics mentioned in Sec. I is to use the operator product expansion at the M_W scale and the renormalization group equations to translate the effective weak theory to more convenient scales ($\mu \sim 2-4$ GeV). At such scales the effective Hamiltonian for $K \to \pi\pi$ decays is the following linear superposition [3]:

$$H_W^{\mathrm{eff}} = \frac{G_F}{\sqrt{2}} V_{ud} V_{us}^* \sum_{i=1}^{10} [z_i(\mu) + \tau y_i(\mu)] O_i(\mu), \tag{1}$$

where z_i and y_i are Wilson coefficients (currently known at two-loop order), $\tau \equiv -V_{td}V_{ts}^*/V_{ud}V_{us}^*$, and O_i are basis of four-fermion operators defined as follows:

$$O_1 = (\bar{s}_\alpha \gamma_\mu (1-\gamma_5) u_\beta)(\bar{u}_\beta \gamma^\mu (1-\gamma_5) d_\alpha), \tag{2a}$$

$$O_2 = (\bar{s}_\alpha \gamma_\mu (1-\gamma_5) u_\alpha)(\bar{u}_\beta \gamma^\mu (1-\gamma_5) d_\beta), \tag{2b}$$

$$O_3 = (\bar{s}_\alpha \gamma_\mu (1-\gamma_5) d_\alpha) \sum_q (\bar{q}_\beta \gamma^\mu (1-\gamma_5) q_\beta), \tag{2c}$$

$$O_4 = (\bar{s}_\alpha \gamma_\mu (1-\gamma_5) d_\beta) \sum_q (\bar{q}_\beta \gamma^\mu (1-\gamma_5) q_\alpha), \tag{2d}$$

$$O_5 = (\bar{s}_\alpha \gamma_\mu (1-\gamma_5) d_\alpha) \sum_q (\bar{q}_\beta \gamma^\mu (1+\gamma_5) q_\beta), \tag{2e}$$

$$O_6 = (\bar{s}_\alpha \gamma_\mu (1-\gamma_5) d_\beta) \sum_q (\bar{q}_\beta \gamma^\mu (1+\gamma_5) q_\alpha), \tag{2f}$$

$$O_7 = \tfrac{3}{2} (\bar{s}_\alpha \gamma_\mu (1-\gamma_5) d_\alpha) \sum_q e_q (\bar{q}_\beta \gamma^\mu (1+\gamma_5) q_\beta), \tag{2g}$$

$$O_8 = \tfrac{3}{2} (\bar{s}_\alpha \gamma_\mu (1-\gamma_5) d_\beta) \sum_q e_q (\bar{q}_\beta \gamma^\mu (1+\gamma_5) q_\alpha), \tag{2h}$$

$$O_9 = \tfrac{3}{2} (\bar{s}_\alpha \gamma_\mu (1-\gamma_5) d_\alpha) \sum_q e_q (\bar{q}_\beta \gamma^\mu (1-\gamma_5) q_\beta), \tag{2i}$$

$$O_{10} = \tfrac{3}{2} (\bar{s}_\alpha \gamma_\mu (1-\gamma_5) d_\beta) \sum_q e_q (\bar{q}_\beta \gamma^\mu (1-\gamma_5) q_\alpha). \tag{2j}$$

Here α and β are color indices, e_q is quark electric charge, and summation is done over all light quarks.

Isospin amplitudes are defined as

$$A_{0,2} e^{i\delta_{0,2}} \equiv \langle (\pi\pi)_{I=0,2} | H_W | K^0 \rangle, \tag{3}$$

where $\delta_{0,2}$ are the final state interaction phases of the two channels. Experimentally

$$\omega = \mathrm{Re}\, A_0 / \mathrm{Re}\, A_2 \simeq 22. \tag{4}$$

The direct CP violation parameter ε' is defined in terms of imaginary parts of these amplitudes:

$$\varepsilon' = -\frac{\mathrm{Im}\, A_0 - \omega\, \mathrm{Im}\, A_2}{\sqrt{2}\, \omega\, \mathrm{Re}\, A_0} e^{i(\pi/2 + \delta_2 - \delta_0)}. \tag{5}$$

Experiments measure the quantity $\mathrm{Re}\,\varepsilon'/\varepsilon$, which is given by

$$\mathrm{Re}\frac{\varepsilon'}{\varepsilon}\simeq\frac{G_F}{2\omega|\varepsilon|\mathrm{Re}\,A_0}\mathrm{Im}\,\lambda_t\,[\Pi_0-\omega\Pi_2], \tag{6}$$

where

$$\Pi_0=\sum_i y_i\langle(\pi\pi)_{I=0}|O_i^{(0)}|K^0\rangle(1-\Omega_{\eta^+\eta'}), \tag{7}$$

$$\Pi_2=\sum_i y_i\langle(\pi\pi)_{I=2}|O_i^{(2)}|K^0\rangle, \tag{8}$$

with $\mathrm{Im}\,\lambda_t\equiv\mathrm{Im}\,V_{td}V_{ts}^*$, and where $\Omega_{\eta^+\eta'}\sim 0.25\pm 0.05$ takes into account the effect of isospin breaking in quark masses ($m_u\neq m_d$). $O_i^{(0)}$ and $O_i^{(2)}$ are isospin 0 and 2 parts of the basis operators. Their expressions are given in Appendix B for completeness.

B. Treatment of charm quark

The effective Hamiltonian given above is obtained in the continuum theory in which the top, bottom, and charm quarks are integrated out. [In particular, the summation in Eqs. (2c)–(2j) is done over *u*, *d*, and *s* quarks.] This makes sense only when the scale μ is sufficiently low compared to the charm quark mass. As mentioned in Ref. [16], at scales comparable to m_c higher-dimensional operators can contribute considerably. Then one should consider an expanded set of operators including those containing the charm quark. Lattice treatment of the charm quark is possible but in practice quite limited, for example by having to work at much smaller lattice spacings and having a more complicated set of operators and contractions. Therefore we have opted to work in the effective theory in which the charm quark is integrated out. Since we typically use $\mu\sim 2$ GeV in our simulations, this falls into a dangerous region. We hope that the effects of higher-dimensional operators can still be neglected, but strictly speaking this issue should be separately investigated.

C. Calculating $\langle\pi\pi|O_i|K^0\rangle$

As was shown by Maiani and Testa [17], two-particle hadronic states are very difficult to construct on the lattice (and in general, in any Euclidean description). We have to use an alternative procedure to calculate the matrix elements appearing in Eqs. (3), (7), and (8). We choose the method [18] in which lowest-order chiral perturbation theory is used to relate $\langle\pi\pi|O_i|K^0\rangle$ to matrix elements involving one-particle states:

$$\langle\pi^+\pi^-|O_i|K^0\rangle=\frac{m_K^2-m_\pi^2}{f}\gamma, \tag{9}$$

$$\langle\pi^+|O_i|K^+\rangle=(p_\pi\cdot p_K)\gamma-\frac{m_s+m_d}{f}\delta, \tag{10}$$

$$\langle 0|O_i|K^0\rangle=(m_s-m_d)\delta, \tag{11}$$

where f is the lowest-order pseudoscalar decay constant. The masses in the first of these formulas are the physical meson masses, while the quark masses and the momenta in the second and third formulas are meant to be from actual simulations on the lattice (done with unphysical masses). These relationships ignore higher-order terms in the chiral expansion, most importantly the final state interactions. Therefore this method suffers from a significant uncertainty. Golterman and Leung [19] have computed one-loop correction for the $\Delta I=3/2$ amplitude in chiral perturbation theory. They find this correction can be large, up to 30% or 60%, depending on the values of unknown contact terms and the cutoff.

III. LATTICE TECHNIQUES

A. Mixing with lower-dimensional operators

Equations (9)–(11) handle unphysical $s\leftrightarrow d$ mixing in $\langle\pi^+|O_i|K^+\rangle$ by subtracting the unphysical part proportional to $\langle 0|O_i|K^0\rangle$. This is equivalent to subtracting the operator

$$O_{\mathrm{sub}}\equiv(m_d+m_s)\bar{s}d+(m_d-m_s)\bar{s}\gamma_5 d. \tag{12}$$

As shown in Refs. [20,21], these statements are also true on the lattice if one uses staggered fermions. A number of Ward identities discussed in these references show that lattice formulation with staggered fermions retains the essential chiral properties of the continuum theory. In particular, O_{sub} defined in Eq. (12) is the only lower-dimensional operator that appears in mixing with the basis operators. (Lower-dimensional operators have to be subtracted nonperturbatively since they are multiplied by powers of a^{-1}.) We employ the nonperturbative procedure suggested in Ref. [21]:

$$\langle\pi^+\pi^-|O_i|K^0\rangle=\langle\pi^+|O_i-\alpha_i O_{\mathrm{sub}}|K^+\rangle\cdot\frac{m_K^2-m_\pi^2}{(p_\pi\cdot p_K)f}, \tag{13}$$

where α_i are found from

$$0=\langle 0|O_i-\alpha_i O_{\mathrm{sub}}|K^0\rangle. \tag{14}$$

This procedure is equivalent to the lattice version of Eqs. (9)–(11) and allows subtraction timeslice by timeslice.

Throughout our simulation we use only degenerate mesons, i.e., $m_s=m_d=m_u$. Since only the negative parity part of O_{sub} contributes in Eq. (14), one naively expects infinity when calculating α_i. However, the matrix elements $\langle 0|O_i|K^0\rangle$ of all basis operators vanish when $m_s=m_d$ due to invariance of both the Lagrangian and all the operators in question under the CPS symmetry, which is defined as the CP symmetry combined with interchange of *s* and *d* quarks. Thus calculation of α_i requires taking the first derivative of $\langle 0|O_i|K^0\rangle$ with respect to (m_d-m_s). In order to evaluate the first derivative numerically, we insert another fermion matrix inversion in turn into all propagators involving the strange quark. Detailed expressions for all contractions are given in the Appendices.

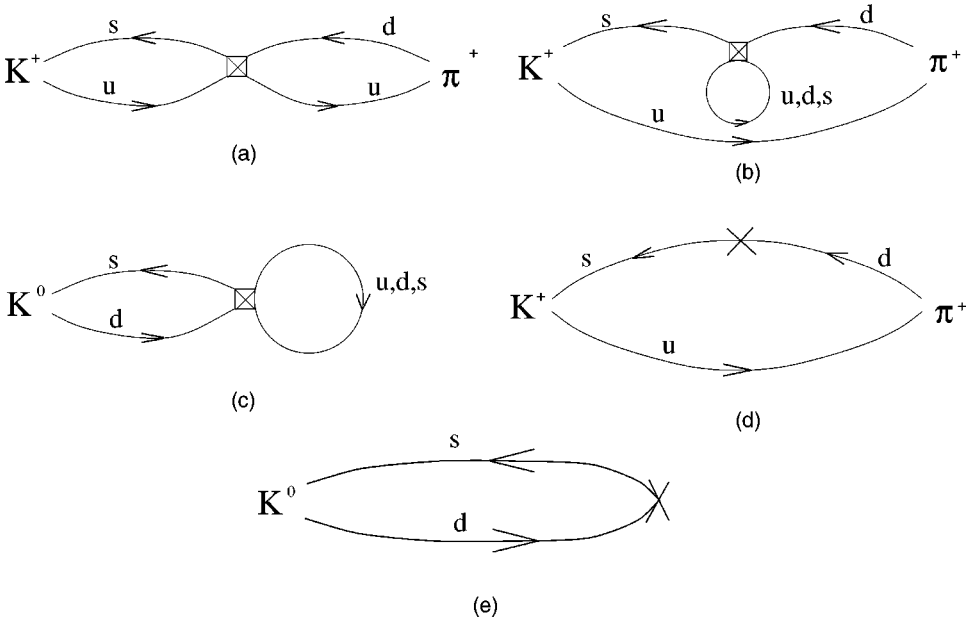

FIG. 1. Five diagram types needed to be computed: (a) ''eight,'' (b) ''eye,'' (c) ''annihilation,'' (d) ''subtraction,'' and (e) two-point function.

B. Diagrams to be computed

According to Eqs. (13) and (14), we need to compute three diagrams involving four-fermion operators (shown in Fig. 1) and a couple of bilinear contractions. The ''eight'' contraction type [Fig. 1(a)] is relatively cheap to compute. It is the only contraction needed for the $\Delta I=3/2$ amplitude. The ''eye'' and ''annihilation'' diagrams [Figs. 1(b) and 1(c)] are much more expensive since they involve calculation of propagators from every point in space-time.

C. Lattice parameters and other details

The parameters of simulation are listed in the Table I. We use periodic boundary conditions in both space and time. Our main ''reference'' ensemble is a set of quenched configurations at $\beta\equiv 6/g^2=6.0$ (Q_1). In addition, we use an ensemble with a larger lattice volume (Q_2), an ensemble with $\beta=6.2$ (Q_3) for checking the lattice spacing dependence, and an ensemble with two dynamical flavors ($m=0.01$) generated by the Columbia group, used for checking the impact of quenching. The quenched ensembles were obtained using a 4-to-1 ratio of 3-hit SU(2) overrelaxed and heatbath algorithms. The configurations were separated by 1000 sweeps. The dynamical configurations were obtained by the *R* algorithm [22].

We use the standard staggered fermion action. Fermion matrices are inverted by the conjugate gradient algorithm. JACKKNIFE is used for statistical analysis.

As explained below, we have extended the lattice four times in the time dimension by copying gauge links. This is done in order to get rid of excited states contamination and wrap-around effects. The largest-volume (Q_2) lattices were extended only two times.

The quenched lattice scale was set as in Ref. [23], i.e., we demand perturbative scaling of the form

$$a(\beta)=a_0\left(\frac{16\pi^2}{11g^2_{\overline{\rm MS}}}\right)^{51/121}\exp\left(\frac{-8\pi^2}{11g^2_{\overline{\rm MS}}}\right), \qquad (15)$$

normalizing so that the world data for the mass of ρ meson [24] is well fit by $m_\rho(a)=(770\ \text{MeV})(1+\Lambda^2a^2(\beta))$. The lattice spacing for the dynamical ensemble is also set by the ρ mass [25].

Some other technicalities are as follows. We work in the two flavor formalism. We use local wall sources that create pseudoscalar mesons at rest. The mesons are degenerate ($m_s=m_d=m_u$, $m_\pi=m_K$). We use staggered fermions and work with gauge-invariant operators, since the gauge symmetry enables significant reduction of the list of possible mixing operators. The staggered flavor structure is assigned depending on the contraction type. Our operators are tadpole improved. This serves to ''improve'' the perturbative expansion at a later stage when we match the lattice and continuum

TABLE I. Simulation parameters.

Ensemble name	N_f	β	Size	a^{-1} (GeV)	L (fm)	Number of configurations	Quark masses used
Q_1	0	6.0	$16^3\times(32\times4)$	2.1	1.6	216	0.01–0.05
Q_2	0	6.0	$32^3\times(64\times2)$	2.1	3.2	26	0.01–0.05
Q_3	0	6.2	$24^3\times(48\times4)$	2.8	1.7	93	0.005–0.03
D	2	5.7	$16^3\times(32\times4)$	2.0	1.6	83	0.01–0.05

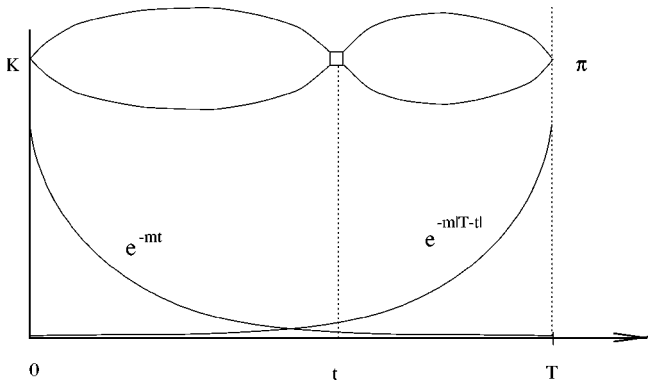

FIG. 2. The general setup of the simulation. An "eight" contraction is shown for convenience. The kaon source is at the timeslice 0, while the pion sink is at the timeslice T. The operator is inserted at a variable time t. The result of this contraction is proportional to the product of two exponentials shown in the figure.

operators. For calculating fermion loops we employ the U(1) pseudofermion stochastic estimator. More details and an explanation of some of these terms can be found in the Appendix A.

D. Setup for calculating matrix elements of four-fermion operators

Consider the setup for calculation of $\langle \pi^+|O_i|K^+\rangle$. Kaons are created at $t_0=0$, the operators are inserted at a variable time t, and the pion sink is located at the time T (see Fig. 2), where T is sufficiently large. In principle, a number of states with pseudoscalar quantum numbers can be created by the kaon source. Each state's contribution is proportional to $\sqrt{Z}e^{-m|t|}$, so the lightest state (kaon) dominates at large enough t. Analogously, states annihilated by the sink contribute proportionally to $\sqrt{Z}e^{-m|T-t|}$, which is dominated by the pion.

In this work kaon and pion have equal mass. In the middle of the lattice, where t is far enough from both 0 and T, we expect to see a plateau, corresponding to $Ze^{-m_\pi T}\langle \pi|O|K\rangle$. This plateau is our working region (see Fig. 3).

As concerns the kaon annihilation matrix elements $\langle 0|O_i|K^0\rangle$, we only need their ratio to $\langle 0|\bar{s}\gamma_5 d|K^0\rangle$, in which the factors $\sqrt{Z}e^{-mt}$ cancel. Indeed, we observe a rather steady plateau (Fig. 4).

E. *B* ratios

It has become conventional to express the results for matrix elements in terms of so-called B ratios, which are the ratios of desired four-fermion matrix elements to their values obtained by vacuum saturation approximation (VSA). For example, the B ratios of operators O_2 and O_4 are formed by dividing the full matrix element by the product of axial-current two-point functions (Fig. 5). We expect the denominator to form a plateau in the middle of the lattice, equal to $Ze^{-m_\pi T}\langle \pi|A_\mu|0\rangle\cdot\langle 0|A^\mu|K\rangle$, where A^μ are the axial vector currents with appropriate flavor quantum numbers for kaon and pion. The factor $Ze^{-m_\pi T}$ cancels, leaving the desirable

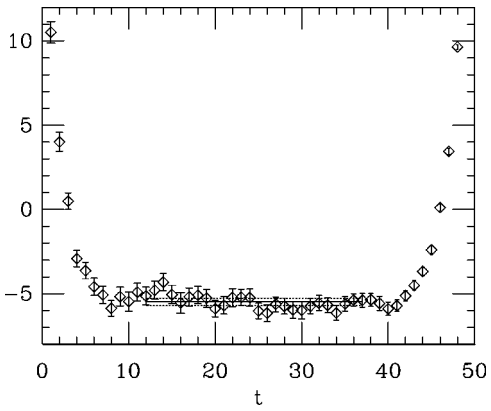

FIG. 3. An example of the signal we get for one of the B ratios (in this case, for the "eye" part of the O_2 operator on the Q_1 ensemble, using quark mass 0.01). The wall sources are at $t=1$ and $t=49$. We see that the excited states quickly disappear and a stable, well-distinguished plateau is observed. We perform JACKKNIFE averaging in the range of t from 12 to 37 (shown with the horizontal lines).

ratio $\langle \pi|O|K\rangle/(\langle \pi|A_\mu|0\rangle\cdot\langle 0|A^\mu|K\rangle)$. Apart from common normalization factors, a number of systematic uncertainties also tend to cancel in this ratio, including the uncertainty in the lattice spacing, quenching, and in some cases perturbative correction uncertainty. Therefore, it is sometimes reasonable to give lattice answers in terms of the B ratios.

However, eventually the physical matrix element needs to be reconstructed by using the known experimental parameters (namely f_K) to compute VSA. In some cases, such as for operators O_5-O_8, the VSA itself is known very imprecisely due to the failure of perturbative matching (see Sec. V). Then it is more reasonable to give answers in terms of matrix elements in physical units. We have adopted the strategy of expressing all matrix elements in units of $\langle \pi|A_\mu|0\rangle\langle 0|A^\mu|K\rangle=(f_K^{\rm latt})^2 m_M^2$ at an intermediate stage, and using precomputed $f_K^{\rm latt}$ at the given meson mass to con-

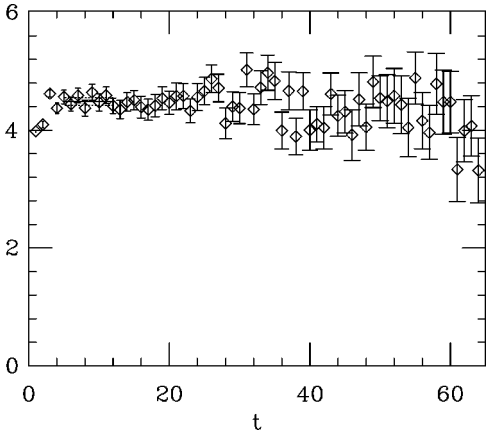

FIG. 4. An example of the signal for $\langle 0|O_2|K^0\rangle/[(m_d-m_s)\langle 0|\bar{s}\gamma_5 d|K^0\rangle]$ on the Q_1 ensemble with quark mass 0.01. The kaon source is at $t=1$. We average over the range of t from 5 to 12 (shown with horizontal lines).

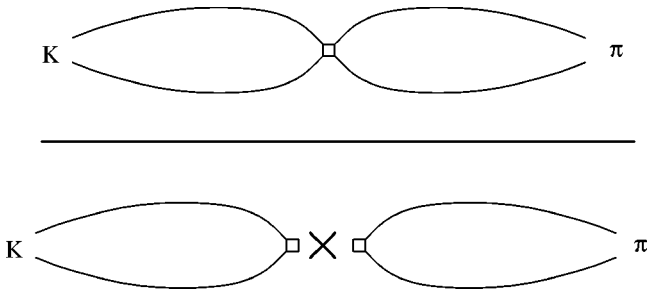

FIG. 5. *B* ratio is formed by dividing the four-fermion matrix element by the product of two-point functions, typically involving A_μ or P bilinears. All the operators involved are inserted at the same timeslice t, and the external meson sources are also located at the same timeslices. This enables cancellation of various common factors.

vert to physical units. This method is sensitive to the choice of the lattice spacing. Our raw results are listed in Tables II–V.

It is very important to check that the time distance between the kaon and pion sources T is large enough so that the excited states do not contribute. That is, the plateau in the middle of the lattice should be sufficiently flat, and the B ratios should not depend on T. We have found that in order to satisfy this requirement the lattice has to be artificially extended in time direction by using a number of copies of the gauge links (four in the case of the small volume lattices, two otherwise). We are using $T=72$ for the Q_3 ($\beta=6.2$) ensemble, and $T=48$ for the rest. An example of a plateau that we obtain with this choice of T is shown in Fig. 3. To read off the result, we average over the whole extension of the plateau, and use JACKKNIFE to estimate the statistical error in this average.

IV. $\Delta I=1/2$ RULE RESULTS

Using the data obtained for matrix elements of basis operators (raw results are listed in Tables II–V), in this section we report numerical results for $\mathrm{Re}\,A_0$ and $\mathrm{Re}\,A_2$ amplitudes as well as their ratio. We discuss these amplitudes separately since the statistics for $\mathrm{Re}\,A_2$ are much better and the continuum limit extrapolation is easier.

A. $\mathrm{Re}\,A_2$ results

The expression for $\mathrm{Re}\,A_2$ can be written as

$$\mathrm{Re}\,A_2=\frac{G_F}{\sqrt{2}}V_{ud}V_{us}^*\,z_+(\mu)\langle O_2(\mu)\rangle_2, \tag{16}$$

where $z_+(\mu)$ is a Wilson coefficient (we use $\mu=2$ GeV) and

$$\langle O_2\rangle_2\equiv\langle(\pi\pi)_{I=2}|O_2^{(2)}|K\rangle. \tag{17}$$

Here

$$\begin{aligned}O_2^{(2)}&=O_1^{(2)}\\&=\tfrac{1}{3}[(\bar{s}\gamma_\mu(1-\gamma_5)u)(\bar{u}\gamma^\mu(1-\gamma_5)d)\\&\quad+(\bar{s}\gamma_\mu(1-\gamma_5)d)(\bar{u}\gamma^\mu(1-\gamma_5)u)\\&\quad-(\bar{s}\gamma_\mu(1-\gamma_5)d)(\bar{d}\gamma^\mu(1-\gamma_5)d)].\end{aligned} \tag{18}$$

In lowest-order chiral perturbation theory the matrix element $\langle O_2\rangle_2$ can be expressed as

$$\langle O_2\rangle_2=\sqrt{2}\frac{m_K^2-m_\pi^2}{f}\,\frac{\langle\pi^+|O_2^{(2)}|K^+\rangle}{m_M^2}. \tag{19}$$

So,

$$\mathrm{Re}\,A_2=G_F\,V_{ud}V_{us}^*\frac{m_K^2-m_\pi^2}{f}R_2, \tag{20}$$

where R_2 is calculated on the lattice and is defined as

$$R_2\equiv z_+\frac{\langle\pi^+|O_2^{(2)}|K^+\rangle}{m_M^2}. \tag{21}$$

The latter matrix element involves only ''eight'' diagrams, and there are no subtractions to be made. Moreover, in the limit of exact $\mathrm{SU}(3)_{\mathrm{flavor}}$ symmetry it is directly related [26] to parameter B_K [which is the B ratio of the neutral kaon mixing operator $O_K=(\bar{s}\gamma_L d)\ (\bar{s}\gamma_L d)$], so that

$$R_2=\tfrac{4}{9}\,z_+(\mu)\,B_K(\mu)\,f_K^2. \tag{22}$$

The parameter B_K is rather well studied (e.g., Refs. [23,27]). Quenched chiral perturbation theory [28] predicts the chiral behavior of the form $B_K=a+bm_K^2+cm_K^2\log m_K^2$, which fits the data well (see Fig. 6) and yields a finite nonzero value in the chiral limit.

The ratio R_2 shows a large dependence on the meson mass used in the simulation (Fig. 7). This is not surprising since both B_K and f_K depend on this mass quite significantly [see Figs. 6 and 8 and Eq. (22)]. Which meson mass should be used to read off the R_2 value for estimation of $\mathrm{Re}\,A_2$ becomes an open question. If known, the higher-order chiral terms would remove this ambiguity. Forced to make a choice, we extrapolate to $M^2=(m_K^2+m_\pi^2)/2$. Using our data for B_K in quenched QCD and taking the continuum limit we obtain $\mathrm{Re}\,A_2=(1.77\pm0.07)\times10^{-8}$ GeV, where the error is only statistical, to be compared with the experimental result $\mathrm{Re}\,A_2=1.23\times10^{-8}$ GeV.

Higher-order chiral terms, including the meson mass dependence, are the largest systematic error in this determination (see analysis in Sec. IV C). Other uncertainties (lattice scale determination, perturbative operator matching, and finite lattice volume) are much smaller.

TABLE II. Raw data for $K\to\pi\pi$ matrix elements: "eights" (E), "eyes" (I) and "annihilation" (A) parts of certain matrix elements, as well as sum total (O) combined by JACKKNIFE for the Q_1 (quenched $\beta=6.0$) ensemble. The notation is explained in the Appendices, and in addition LR means $VA-AV$. The data are in units of $\langle\pi|A_\mu|0\rangle\cdot\langle 0|A^\mu|K\rangle$. Lattice results for meson decay constant f are also shown (in units of $1/a$) in order to allow translation into physical units.

Quark mass	$m=0.01$	$m=0.02$	$m=0.03$	$m=0.04$	$m=0.05$
$N_{\rm conf}$	216	216	216	23	23
AA_{EU}	1.499±0.018	1.208±0.007	1.129±0.004	1.075±0.007	1.056±0.010
AA_{EF}	1.465±0.040	0.718±0.011	0.522±0.005	0.427±0.008	0.388±0.005
VV_{EU}	−0.341±0.015	−0.100±0.003	−0.045±0.002	−0.025±0.004	−0.019±0.003
VV_{EF}	−1.709±0.039	−0.838±0.012	−0.559±0.005	−0.399±0.010	−0.325±0.007
SS_{EU}	−6.610±0.100	−1.933±0.023	−0.891±0.009	−0.471±0.010	−0.307±0.006
SS_{EF}	−6.592±0.075	−2.042±0.017	−0.989±0.006	−0.547±0.007	−0.360±0.004
PP_{EU}	−263.040±2.312	−123.693±0.735	−81.633±0.331	−60.735±0.606	−48.990±0.424
PP_{EF}	−113.141±0.995	−52.578±0.311	−34.491±0.139	−25.562±0.252	−20.572±0.176
LR_{EU}	0.005±0.001	0.006±0.000	0.006±0.000	0.005±0.001	0.005±0.001
LR_{EF}	0.064±0.003	0.097±0.003	0.108±0.002	0.107±0.005	0.108±0.008
AA_{IU}	0.421±0.038	0.292±0.016	0.211±0.010	0.130±0.015	0.108±0.012
AA_{IF}	0.860±0.062	0.601±0.022	0.422±0.012	0.298±0.020	0.243±0.017
VV_{IU}	−0.107±0.039	−0.029±0.017	−0.030±0.010	−0.017±0.016	−0.010±0.011
VV_{IF}	−6.356±0.261	−4.900±0.121	−3.715±0.073	−2.840±0.118	−2.331±0.160
SS_{IU}	−240.110±4.887	−148.609±2.487	−108.522±1.659	−80.907±2.847	−68.255±3.475
SS_{IF}	−101.939±2.078	−62.536±1.046	−45.511±0.695	−33.910±1.198	−28.561±1.456
PP_{IU}	−3.277±0.088	−0.982±0.024	−0.456±0.010	−0.254±0.016	−0.156±0.012
PP_{IF}	−3.538±0.093	−1.113±0.021	−0.552±0.011	−0.324±0.012	−0.207±0.011
AV_{A1U}	−0.117±0.021	−0.062±0.012	−0.025±0.009	−0.011±0.026	−0.012±0.028
AV_{A1F}	−5.390±0.096	−4.789±0.043	−4.323±0.021	−3.946±0.043	−3.647±0.036
VA_{A1U}	0.416±0.025	0.287±0.011	0.225±0.008	0.158±0.021	0.163±0.012
VA_{A1F}	0.895±0.029	0.610±0.012	0.489±0.008	0.421±0.021	0.368±0.014
AV_{A2U}	0.001±0.012	0.005±0.005	0.002±0.003	−0.012±0.006	0.011±0.005
AV_{A2F}	−0.026±0.018	0.002±0.005	0.002±0.003	−0.002±0.006	0.004±0.004
VA_{A2U}	−0.000±0.012	0.001±0.004	−0.001±0.002	0.001±0.005	0.001±0.004
VA_{A2F}	0.020±0.015	0.001±0.005	−0.001±0.003	−0.000±0.006	0.003±0.004
SP_{A2U}	0.176±0.021	0.033±0.006	0.005±0.003	0.003±0.005	0.003±0.004
SP_{A2F}	0.081±0.017	−0.031±0.005	−0.040±0.002	−0.033±0.005	−0.024±0.003
PS_{A2U}	−85.827±0.278	−81.799±0.116	−77.678±0.081	−73.540±0.149	−69.678±0.113
PS_{A2F}	−35.680±0.122	−34.081±0.050	−32.381±0.034	−30.664±0.062	−29.058±0.049
$O_1^{1/2}$	−0.726±0.067	−0.480±0.031	−0.418±0.018	−0.344±0.025	−0.320±0.036
$O_1^{3/2}$	0.304±0.004	0.329±0.002	0.349±0.001	0.360±0.003	0.367±0.004
$O_2^{1/2}$	2.732±0.272	1.931±0.077	1.522±0.034	1.146±0.059	1.060±0.051
$O_2^{3/2}$	0.304±0.004	0.329±0.002	0.349±0.001	0.360±0.003	0.367±0.004
$O_3^{1/2}$	2.989±0.551	2.082±0.172	1.437±0.092	0.912±0.130	0.781±0.159
$O_4^{1/2}$	6.447±0.807	4.493±0.234	3.377±0.112	2.402±0.178	2.161±0.178
$O_5^{1/2}$	−26.059±2.016	−16.133±0.646	−12.336±0.346	−9.918±0.588	−7.353±0.625
$O_6^{1/2}$	−55.625±4.975	−35.402±1.546	−26.976±0.849	−22.268±1.365	−16.426±1.495
$O_7^{1/2}$	92.079±0.917	41.611±0.327	26.709±0.163	19.512±0.319	15.977±0.325
$O_7^{3/2}$	54.195±0.469	25.922±0.151	17.338±0.069	13.057±0.123	10.644±0.089
$O_8^{1/2}$	222.384±2.214	100.967±0.780	65.237±0.394	47.858±0.761	39.424±0.784
$O_8^{3/2}$	129.802±1.122	61.658±0.362	40.911±0.164	30.545±0.295	24.698±0.212
$O_9^{1/2}$	−2.584±0.272	−1.761±0.077	−1.346±0.034	−0.972±0.060	−0.870±0.052
$O_9^{3/2}$	0.456±0.006	0.494±0.003	0.523±0.002	0.539±0.005	0.550±0.005
$O_{10}^{1/2}$	0.8747±0.071	0.650±0.031	0.594±0.019	0.518±0.023	0.510±0.037
$O_{10}^{3/2}$	0.456±0.006	0.494±0.003	0.523±0.002	0.539±0.005	0.550±0.005
f	$(627\pm11)\times10^{-4}$	$(739\pm21)\times10^{-4}$	$(828\pm11)\times10^{-4}$	$(928\pm16)\times10^{-4}$	$(1153\pm24)\times10^{-4}$

TABLE III. Raw data for $K\to\pi\pi$ matrix elements: "eights" (E), "eyes" (I), and "annihilation" (A) parts as well as sum total (O) combined by JACKKNIFE for the Q_2 ($\beta=6.0$, higher volume) ensemble. The data are in units of $\langle\pi|A_\mu|0\rangle\cdot\langle 0|A^\mu|K\rangle$. Lattice results for meson decay constant f are also shown (in units of $1/a$) in order to allow translation into physical units.

Quark mass	$m=0.01$	$m=0.02$	$m=0.03$	$m=0.04$	$m=0.05$
$N_{\rm conf}$	26	26	26	26	26
AA_{EU}	1.326±0.036	1.193±0.031	1.105±0.003	1.073±0.002	1.042±0.019
AA_{EF}	0.927±0.040	0.605±0.019	0.482±0.004	0.416±0.002	0.380±0.007
VV_{EU}	−0.145±0.010	−0.058±0.003	−0.034±0.001	−0.021±0.001	−0.015±0.001
VV_{EF}	−1.203±0.041	−0.735±0.022	−0.522±0.005	−0.402±0.003	−0.322±0.006
SS_{EU}	−6.700±0.225	−2.021±0.057	−0.904±0.007	−0.500±0.003	−0.306±0.006
SS_{EF}	−6.670±0.206	−2.122±0.055	−0.990±0.004	−0.571±0.002	−0.360±0.006
PP_{EU}	−262.478±7.257	−125.277±3.053	−80.496±0.203	−60.811±0.146	−48.791±0.857
PP_{EF}	−112.841±3.122	−53.246±1.301	−34.006±0.085	−25.595±0.061	−20.485±0.360
LR_{EU}	0.001±0.000	0.001±0.000	0.005±0.000	0.006±0.000	0.001±0.000
LR_{EF}	0.008±0.000	0.012±0.000	0.103±0.002	0.106±0.002	0.013±0.000
AA_{IU}	0.478±0.034	0.302±0.020	0.183±0.011	0.143±0.005	0.103±0.004
AA_{IF}	0.992±0.059	0.638±0.024	0.395±0.010	0.304±0.006	0.222±0.007
VV_{IU}	−0.168±0.041	−0.054±0.020	−0.021±0.011	−0.028±0.006	−0.019±0.005
VV_{IF}	−6.694±0.209	−4.955±0.108	−3.561±0.069	−2.818±0.056	−2.214±0.038
SS_{IU}	−243.216±3.839	−150.952±2.618	−104.282±1.475	−81.935±1.457	−65.920±0.866
SS_{IF}	−103.122±1.644	−63.477±1.103	−43.720±0.617	−34.295±0.611	−27.586±0.362
PP_{IU}	−3.138±0.078	−1.004±0.025	−0.462±0.011	−0.247±0.008	−0.163±0.004
PP_{IF}	−3.373±0.082	−1.147±0.030	−0.557±0.008	−0.330±0.009	−0.213±0.003
AV_{A1U}	−0.097±0.042	−0.053±0.018	−0.037±0.011	−0.020±0.008	−0.004±0.007
AV_{A1F}	−5.294±0.102	−4.690±0.039	−4.348±0.026	−3.978±0.017	−3.659±0.013
VA_{A1U}	0.418±0.037	0.271±0.013	0.221±0.009	0.198±0.009	0.150±0.005
VA_{A1F}	0.824±0.042	0.597±0.016	0.468±0.010	0.402±0.009	0.336±0.005
AV_{A2U}	−0.038±0.021	0.003±0.007	−0.002±0.004	0.002±0.003	−0.001±0.002
AV_{A2F}	−0.006±0.028	−0.011±0.010	−0.004±0.005	0.005±0.002	−0.003±0.002
VA_{A2U}	−0.027±0.017	0.006±0.005	0.001±0.003	0.002±0.002	−0.001±0.002
VA_{A2F}	−0.014±0.020	0.008±0.006	−0.002±0.004	−0.004±0.002	0.000±0.002
SP_{A2U}	0.154±0.021	0.033±0.007	0.001±0.004	−0.006±0.002	−0.007±0.001
SP_{A2F}	0.039±0.015	−0.036±0.006	−0.047±0.003	−0.039±0.002	−0.032±0.001
PS_{A2U}	−85.672±0.221	−81.961±0.168	−77.765±0.050	−73.718±0.039	−69.916±0.033
PS_{A2F}	−35.660±0.100	−34.159±0.071	−32.429±0.021	−30.747±0.016	−29.164±0.013
$O_1^{1/2}$	−0.800±0.090	−0.503±0.043	−0.411±0.020	−0.378±0.014	−0.378±0.014
$O_1^{3/2}$	0.302±0.009	0.335±0.009	0.343±0.001	0.355±0.001	0.355±0.001
$O_2^{1/2}$	2.576±0.189	1.878±0.079	1.521±0.031	1.258±0.025	1.258±0.025
$O_2^{3/2}$	0.302±0.009	0.335±0.009	0.343±0.001	0.355±0.001	0.355±0.001
$O_3^{1/2}$	2.591±0.503	1.903±0.187	1.472±0.098	1.021±0.063	1.021±0.063
$O_4^{1/2}$	5.967±0.626	4.284±0.241	3.404±0.112	2.657±0.077	2.657±0.077
$O_5^{1/2}$	−24.182±3.520	−16.199±1.122	−12.605±0.318	−9.853±0.297	−9.853±0.297
$O_6^{1/2}$	−52.364±8.362	−35.350±2.815	−27.803±0.805	−21.773±0.716	−21.773±0.716
$O_7^{1/2}$	93.034±1.444	42.292±0.777	26.055±0.135	19.526±0.141	19.526±0.141
$O_7^{3/2}$	53.821±1.480	26.188±0.640	17.078±0.041	13.059±0.030	13.059±0.030
$O_8^{1/2}$	224.874±3.524	102.848±1.887	63.749±0.320	48.048±0.339	48.048±0.339
$O_8^{3/2}$	128.954±3.550	62.298±1.519	40.298±0.099	30.564±0.072	30.564±0.072
$O_9^{1/2}$	−2.496±0.196	−1.706±0.082	−1.353±0.031	−1.078±0.024	−1.078±0.024
$O_9^{3/2}$	0.453±0.013	0.503±0.013	0.515±0.002	0.533±0.001	0.533±0.001
$O_{10}^{1/2}$	0.880±0.102	0.675±0.043	0.580±0.018	0.558±0.014	0.558±0.014
$O_{10}^{3/2}$	0.453±0.013	0.503±0.013	0.515±0.002	0.533±0.001	0.533±0.001
f	$(730\pm8)\times10^{-4}$	$(851\pm5)\times10^{-4}$	$(966\pm8)\times10^{-4}$	$(1073\pm7)\times10^{-4}$	$(1176\pm7)\times10^{-4}$

TABLE IV. Raw data for $K\to\pi\pi$ matrix elements: "eights" (E), "eyes" (I), and "annihilation" (A) parts as well as sum total (O) combined by JACKKNIFE for the Q_3 ($\beta=6.2$) ensemble. The data are in units of $\langle\pi|A_\mu|0\rangle\cdot\langle 0|A^\mu|K\rangle$. Lattice results for meson decay constant f are also shown (in units of $1/a$) in order to allow translation into physical units.

Quark mass	$m=0.005$	$m=0.01$	$m=0.015$	$m=0.02$	$m=0.03$
$N_{\rm conf}$	93	93	93	93	92
AA_{EU}	1.858±0.040	1.432±0.019	1.254±0.012	1.209±0.009	1.127±0.006
AA_{EF}	2.514±0.131	1.228±0.039	0.771±0.017	0.666±0.011	0.500±0.006
VV_{EU}	−0.647±0.044	−0.227±0.014	−0.098±0.007	−0.071±0.004	−0.032±0.002
VV_{EF}	−2.970±0.105	−1.583±0.041	−1.013±0.019	−0.838±0.014	−0.577±0.008
SS_{EU}	−26.445±0.740	−8.394±0.191	−3.913±0.071	−2.280±0.038	−1.004±0.013
SS_{EF}	−21.265±0.511	−7.022±0.121	−3.431±0.046	−2.064±0.025	−0.968±0.008
PP_{EU}	−421.688±6.876	−190.010±2.146	−120.956±1.050	−89.033±0.658	−59.246±0.279
PP_{EF}	−186.537±3.188	−83.104±0.975	−52.194±0.478	−38.418±0.287	−25.380±0.120
LR_{EU}	0.004±0.001	0.008±0.001	0.012±0.001	0.012±0.001	0.013±0.001
LR_{EF}	0.077±0.008	0.155±0.007	0.206±0.011	0.235±0.009	0.265±0.007
AA_{IU}	0.651±0.126	0.648±0.055	0.556±0.041	0.421±0.024	0.307±0.011
AA_{IF}	1.313±0.172	1.224±0.072	1.073±0.057	0.903±0.042	0.656±0.021
VV_{IU}	−0.036±0.112	−0.011±0.052	−0.108±0.035	−0.076±0.025	−0.042±0.012
VV_{IF}	−11.387±1.081	−11.235±0.432	−10.047±0.481	−8.612±0.300	−6.758±0.172
SS_{IU}	−424.398±12.231	−307.683±7.808	−258.961±9.757	−212.161±6.490	−164.611±3.885
SS_{IF}	−182.319±5.323	−130.996±3.329	−109.181±4.056	−89.852±2.717	−69.605±1.632
PP_{IU}	−11.640±0.467	−3.821±0.127	−1.958±0.086	−1.165±0.042	−0.562±0.017
PP_{IF}	−9.974±0.381	−3.501±0.102	−1.965±0.079	−1.188±0.038	−0.628±0.014
AV_{A1U}	−0.103±0.031	−0.054±0.016	−0.037±0.015	−0.045±0.013	−0.036±0.010
AV_{A1F}	−4.484±0.249	−4.054±0.099	−3.924±0.054	−3.813±0.032	−3.600±0.018
VA_{A1U}	0.407±0.033	0.233±0.017	0.222±0.013	0.194±0.011	0.160±0.008
VA_{A1F}	0.782±0.053	0.508±0.022	0.430±0.013	0.407±0.010	0.352±0.007
AV_{A2U}	−0.020±0.012	0.006±0.004	0.003±0.002	0.001±0.002	−0.000±0.001
AV_{A2F}	−0.021±0.026	0.005±0.006	0.002±0.003	0.000±0.002	0.000±0.001
VA_{A2U}	0.009±0.015	−0.005±0.004	0.005±0.002	−0.000±0.001	−0.000±0.001
VA_{A2F}	0.042±0.019	−0.003±0.005	−0.004±0.003	0.003±0.002	−0.001±0.001
SP_{A2U}	0.516±0.048	0.135±0.014	0.031±0.007	−0.007±0.004	−0.027±0.002
SP_{A2F}	0.287±0.032	0.026±0.010	−0.041±0.005	−0.063±0.002	−0.065±0.001
PS_{A2U}	−75.099±0.315	−75.664±0.130	−74.992±0.072	−73.901±0.046	−71.282±0.027
PS_{A2F}	−31.270±0.145	−31.802±0.073	−31.396±0.056	−31.133±0.047	−30.041±0.045
$O_1^{1/2}$	−1.129±0.203	−0.561±0.081	−0.629±0.053	−0.517±0.044	−0.401±0.023
$O_1^{3/2}$	0.252±0.010	0.283±0.003	0.305±0.003	0.322±0.002	0.339±0.002
$O_2^{1/2}$	3.477±1.315	1.948±0.439	1.883±0.228	1.502±0.105	1.220±0.051
$O_2^{3/2}$	0.252±0.010	0.283±0.003	0.305±0.003	0.322±0.002	0.339±0.002
$O_3^{1/2}$	3.279±2.473	1.921±0.860	1.558±0.483	1.121±0.260	0.898±0.120
$O_4^{1/2}$	7.885±3.815	4.429±1.293	4.070±0.693	3.139±0.336	2.519±0.157
$O_5^{1/2}$	−32.000±4.403	−18.586±1.769	−13.684±1.376	−11.871±0.717	−7.526±0.420
$O_6^{1/2}$	−68.245±11.915	−40.623±4.435	−28.721±3.468	−26.246±1.750	−16.554±0.965
$O_7^{1/2}$	146.448±2.604	65.609±0.959	41.127±0.621	29.642±0.348	19.999±0.200
$O_7^{3/2}$	83.888±1.363	38.871±0.437	25.057±0.221	18.817±0.135	12.786±0.059
$O_8^{1/2}$	350.563±5.938	157.286±2.201	99.768±1.502	71.553±0.874	48.564±0.479
$O_8^{3/2}$	200.364±3.133	92.214±1.001	59.413±0.497	44.128±0.317	29.660±0.137
$O_9^{1/2}$	−3.333±1.316	−1.801±0.440	−1.722±0.229	−1.335±0.106	−1.051±0.051
$O_9^{3/2}$	0.378±0.014	0.424±0.005	0.457±0.004	0.483±0.003	0.509±0.002
$O_{10}^{1/2}$	1.273±0.213	0.707±0.082	0.789±0.054	0.683±0.045	0.570±0.023
$O_{10}^{3/2}$	0.378±0.014	0.424±0.005	0.457±0.004	0.483±0.003	0.509±0.002
f	$(407\pm5)\times10^{-4}$	$(451\pm4)\times10^{-4}$	$(492\pm4)\times10^{-4}$	$(536\pm4)\times10^{-4}$	$(611\pm4)\times10^{-4}$

TABLE V. Raw data for $K\to\pi\pi$ matrix elements: "eights" (E), "eyes" (I), and "annihilation" (A) parts as well as sum total (O) combined by JACKKNIFE for the D ($N_f=2$, $\beta=5.7$) ensemble. The data are in units of $\langle\pi|A_\mu|0\rangle\cdot\langle 0|A^\mu|K\rangle$. Lattice results for meson decay constant f are also shown (in units of $1/a$) in order to allow translation into physical units.

Quark mass	$m=0.01$	$m=0.02$	$m=0.03$	$m=0.04$	$m=0.05$
$N_{\rm conf}$	83	83	32	33	33
AA_{EU}	1.593±0.039	1.233±0.014	1.133±0.013	1.087±0.009	1.062±0.006
AA_{EF}	1.595±0.088	0.738±0.016	0.508±0.012	0.425±0.007	0.384±0.004
VV_{EU}	−0.375±0.031	−0.115±0.006	−0.049±0.004	−0.028±0.002	−0.018±0.001
VV_{EF}	−1.867±0.084	−0.820±0.019	−0.515±0.015	−0.377±0.009	−0.300±0.005
SS_{EU}	−5.520±0.192	−1.435±0.032	−0.625±0.018	−0.346±0.008	−0.215±0.005
SS_{EF}	−5.937±0.151	−1.659±0.027	−0.775±0.015	−0.448±0.007	−0.289±0.004
PP_{EU}	−289.852±5.473	−129.095±1.377	−85.485±1.009	−64.048±0.570	−51.605±0.373
PP_{EF}	−125.605±2.369	−55.361±0.590	−36.469±0.428	−27.245±0.240	−21.911±0.157
LR_{EU}	0.002±0.001	0.004±0.000	0.003±0.001	0.002±0.000	0.002±0.000
LR_{EF}	0.040±0.003	0.059±0.003	0.059±0.004	0.056±0.003	0.052±0.002
AA_{IU}	0.483±0.082	0.378±0.033	0.193±0.036	0.123±0.017	0.095±0.015
AA_{IF}	1.022±0.104	0.723±0.046	0.438±0.041	0.306±0.020	0.216±0.015
VV_{IU}	0.023±0.094	−0.075±0.040	−0.030±0.035	−0.026±0.017	−0.020±0.014
VV_{IF}	−8.735±0.742	−6.268±0.259	−4.314±0.280	−3.136±0.162	−2.374±0.106
SS_{IU}	−294.011±11.938	−167.898±4.893	−115.824±5.170	−86.549±3.057	−68.230±2.059
SS_{IF}	−125.822±5.060	−71.428±2.086	−49.094±2.189	−36.664±1.293	−28.897±0.871
PP_{IU}	−2.590±0.135	−0.761±0.038	−0.299±0.029	−0.192±0.013	−0.120±0.012
PP_{IF}	−3.015±0.131	−0.965±0.045	−0.492±0.039	−0.294±0.017	−0.185±0.012
AV_{A1U}	−0.102±0.030	−0.055±0.021	−0.047±0.027	−0.031±0.017	−0.036±0.021
AV_{A1F}	−6.464±0.156	−5.606±0.052	−4.999±0.047	−4.523±0.031	−4.090±0.020
VA_{A1U}	0.488±0.034	0.305±0.020	0.217±0.026	0.189±0.016	0.154±0.014
VA_{A1F}	1.012±0.036	0.672±0.022	0.576±0.025	0.471±0.013	0.382±0.012
AV_{A2U}	−0.012±0.016	0.001±0.008	−0.001±0.009	−0.002±0.006	−0.006±0.005
AV_{A2F}	−0.014±0.024	−0.007±0.008	0.010±0.009	0.004±0.006	0.005±0.006
VA_{A2U}	−0.010±0.016	0.011±0.006	0.002±0.007	−0.000±0.003	0.002±0.003
VA_{A2F}	0.012±0.020	0.004±0.008	0.004±0.009	−0.000±0.004	−0.003±0.005
SP_{A2U}	−0.009±0.031	−0.055±0.007	−0.045±0.006	−0.035±0.003	−0.024±0.002
SP_{A2F}	−0.102±0.028	−0.123±0.006	−0.094±0.006	−0.068±0.003	−0.050±0.002
PS_{A2U}	−99.624±0.485	−92.338±0.199	−85.628±0.182	−79.897±0.121	−74.801±0.090
PS_{A2F}	−42.080±0.213	−39.033±0.087	−36.209±0.078	−33.783±0.052	−31.632±0.038
$O_1^{1/2}$	−0.886±0.139	−0.482±0.068	−0.387±0.070	−0.359±0.036	−0.300±0.028
$O_1^{3/2}$	0.315±0.011	0.345±0.004	0.359±0.004	0.369±0.003	0.376±0.002
$O_2^{1/2}$	4.558±0.621	2.304±0.139	1.611±0.097	1.327±0.061	1.137±0.042
$O_2^{3/2}$	0.315±0.011	0.345±0.004	0.359±0.004	0.369±0.003	0.376±0.002
$O_3^{1/2}$	6.193±1.236	2.802±0.318	1.686±0.291	1.205±0.171	0.998±0.126
$O_4^{1/2}$	11.636±1.833	5.588±0.419	3.683±0.327	2.891±0.204	2.435±0.144
$O_5^{1/2}$	−46.800±3.109	−24.184±1.182	−16.060±0.834	−11.625±0.550	−8.890±0.433
$O_6^{1/2}$	−99.356±7.610	−52.041±2.682	−34.328±1.825	−25.144±1.227	−19.409±0.956
$O_7^{1/2}$	94.131±1.816	40.842±0.582	26.982±0.442	20.369±0.275	16.607±0.192
$O_7^{3/2}$	60.818±1.141	27.525±0.290	18.438±0.213	13.956±0.121	11.351±0.079
$O_8^{1/2}$	224.179±4.337	97.842±1.388	65.310±1.079	49.484±0.673	40.473±0.474
$O_8^{3/2}$	143.897±2.705	64.609±0.686	42.941±0.506	32.252±0.285	26.037±0.186
$O_9^{1/2}$	−4.425±0.623	−2.125±0.141	−1.423±0.097	−1.142±0.061	−0.949±0.043
$O_9^{3/2}$	0.473±0.016	0.518±0.005	0.539±0.006	0.554±0.004	0.563±0.003
$O_{10}^{1/2}$	1.019±0.145	0.662±0.070	0.575±0.073	0.545±0.037	0.487±0.029
$O_{10}^{3/2}$	0.473±0.016	0.518±0.005	0.539±0.006	0.554±0.004	0.563±0.003
f	$(541\pm11)\times10^{-4}$	$(676\pm10)\times10^{-4}$	$(800\pm9)\times10^{-4}$	$(936\pm12)\times10^{-4}$	$(1035\pm14)\times10^{-4}$

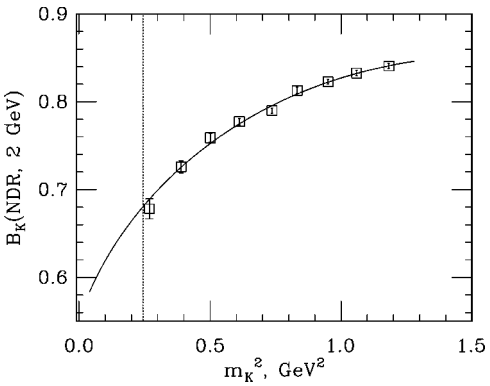

FIG. 6. Parameter B_K in NDR $\overline{\text{MS}}$ scheme at 2 GeV on the dynamical ensemble vs the meson mass squared. The fit is of the form $B_K=a+bm_K^2+cm_K^2\log m_K^2$. The vertical line here and in the other plots below marks the physical kaon mass.

B. Re A_0 results

Using Eqs. (13) and (14), Re A_0 can be expressed as

$$\mathrm{Re}\,A_0=\frac{G_F}{\sqrt{2}}V_{ud}V_{us}^*\frac{m_K^2-m_\pi^2}{f}R_0, \tag{23}$$

where

$$R_0\equiv\sum_i z_i\frac{\langle\pi^+|O_i^{(0)}|K^+\rangle_s}{m^2}.$$

Here z_i are Wilson coefficients, and the subscript "s" indicates that these matrix elements already include subtraction of $\langle\pi^+|O_{\rm sub}|K^+\rangle$. $O_i^{(0)}$ are isospin 0 parts of operators O_i (given in Appendix B for completeness). For example,

$$\begin{aligned}O_1^{(0)}=&\tfrac{2}{3}(\bar{s}\gamma_\mu(1-\gamma_5)d)(\bar{u}\gamma^\mu(1-\gamma_5)u)\\&-\tfrac{1}{3}(\bar{s}\gamma_\mu(1-\gamma_5)u)(\bar{u}\gamma^\mu(1-\gamma_5)d)\\&+\tfrac{1}{3}(\bar{s}\gamma_\mu(1-\gamma_5)d)(\bar{d}\gamma^\mu(1-\gamma_5)d),\end{aligned} \tag{24}$$

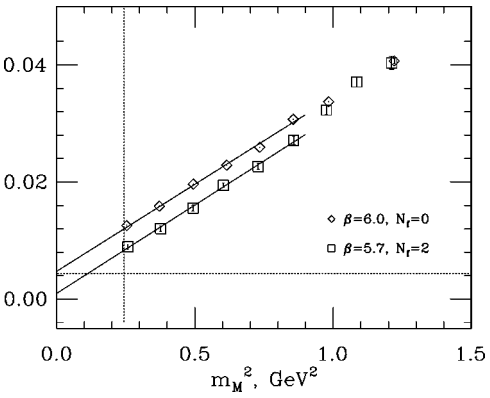

FIG. 7. Matrix element R_2 computed on the dynamical D (squares) and quenched Q_1 (diamonds) ensembles. Re A_2 is proportional to this quantity in the lowest order in chiral perturbation theory. The horizontal line shows the value corresponding to the experiment.

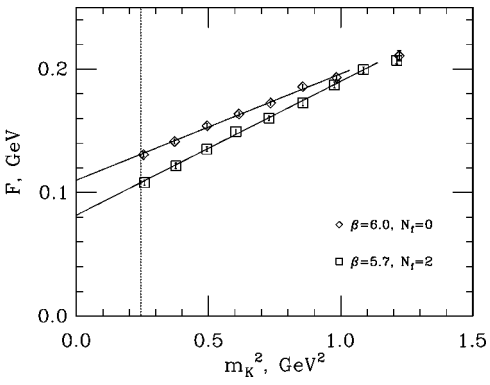

FIG. 8. Pseudoscalar decay constant ($F_\pi=93$ MeV in continuum) on the dynamical D (squares) and quenched Q_1 (diamonds) ensembles vs meson mass squared.

$$\begin{aligned}O_2^{(0)}=&\tfrac{2}{3}(\bar{s}\gamma_\mu(1-\gamma_5)u)(\bar{u}\gamma^\mu(1-\gamma_5)d)\\&-\tfrac{1}{3}(\bar{s}\gamma_\mu(1-\gamma_5)d)(\bar{u}\gamma^\mu(1-\gamma_5)u)+\tfrac{1}{3}(\bar{s}\gamma_\mu(1\\&-\gamma_5)d)(\bar{d}\gamma^\mu(1-\gamma_5)d).\end{aligned} \tag{25}$$

All contraction types are needed (as opposed to the calculation of Re A_2), including the expensive "eyes" and "annihilations." The results for quenched $\beta=6.0$ and $\beta=6.2$ ensembles are shown in Fig. 9. Dependence of R_0 on the meson mass is small, so there is no big ambiguity about the mass prescription as in the R_2 case. Considerable cutoff dependence is present (Fig. 10).

We have checked the lattice volume dependence by comparing ensembles Q_1 and Q_2 (1.6 and 3.2 fm at $\beta=6.0$). The dependence was found to be small, so we consider $(1.6\ \text{fm})^3$ as a volume large enough to contain the system. We have also checked the effect of quenching and found it to be small compared to noise (see Fig. 11). In addition, there is an operator matching uncertainty coming from mixing of O_2 with O_6 operators through penguin diagrams in lattice perturba-

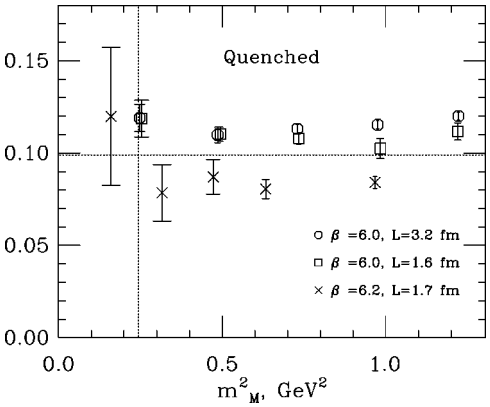

FIG. 9. Matrix element R_0 for quenched ensembles plotted against the meson mass squared. Re A_0 is proportional to this quantity in the lowest order in chiral perturbation theory. The upper group of points is for ensembles Q_1 and Q_2, while the lower group is for Q_3. Only statistical errors are shown. The horizontal line shows the value corresponding to the experiment.

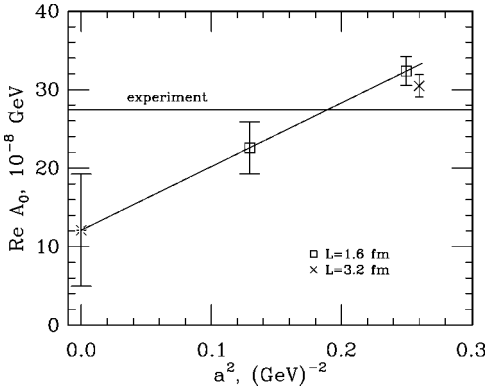

FIG. 10. $\mathrm{Re}\,A_0$ for quenched ensembles plotted against lattice spacing squared. A naive extrapolation to the continuum limit is made. The horizontal line corresponds to the experimental result of 27.8×10^{-8} GeV. Only statistical errors are shown.

tion theory. This is explained in Sec. V A. We estimate that this uncertainty does not exceed 20% for all ensembles.

The breakdown of contributions of various basis operators to $\mathrm{Re}\,A_0$ is shown in Fig. 12. By far, O_2 plays the most important role, whereas penguins have only a small influence.

C. $\Delta I=1/2$ rule results and errors

Shown in Fig. 13 is the ratio $\mathrm{Re}\,A_2/\mathrm{Re}\,A_0$ as directly computed on the lattice for quenched and dynamical data sets. The data exhibit strong dependence on the meson mass, primarily due to the chiral behavior of $\mathrm{Re}\,A_2$ (compare with Fig. 7). Taking the meson mass as $m_K/\sqrt{2}$ we obtain

$$\frac{\mathrm{Re}\,A_2}{\mathrm{Re}\,A_0}=0.044\pm0.010\ \ (\mathrm{stat})\ \pm0.024\ \ (\mathrm{syst}). \qquad (26)$$

The central value is based on the dynamical $\beta=5.7$ results.

The predominant source of systematic error in this ratio is higher-order chiral terms. Unfortunately a rigorous study of these terms is impossible at present because they involve a cutoff parameter Λ which is known only approximately, and the higher-order momentum expansion (contact terms) parameters are not known at all. Various combinations of these

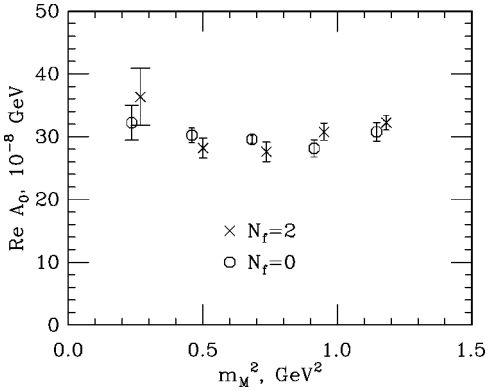

FIG. 11. Comparison of quenched (Q_1) and dynamical results for $\mathrm{Re}\,A_0$ at comparable lattice spacings.

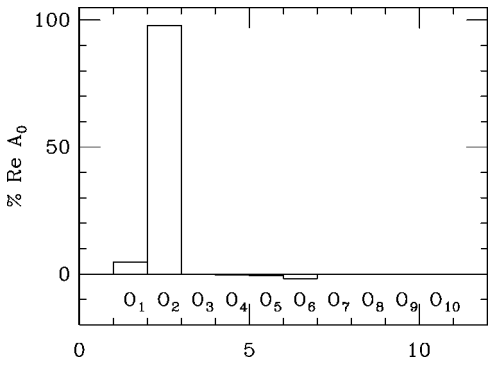

FIG. 12. Contribution of various operators to $\mathrm{Re}\,A_0$.

unknowns can lead to vastly different results. So we can only estimate the order of magnitude of higher-order chiral terms, for example by choosing a reasonable value for Λ and evaluating only chiral logs (setting the contact terms to zero).

For $\Delta I=1/2$ amplitude, the final state interactions tend to increase $\mathrm{Re}\,A_0$ by about 30%, according to Ref. [29]. The one-loop chiral corrections also change the relative weights of $K\to\pi$ and $K\to0$ matrix elements, and since these two contributions have different signs, the total $\mathrm{Re}\,A_0$ amplitude is extremely sensitive to these corrections. It tends to decrease considerably after the one-loop corrections have been put in.

For the $\Delta I=3/2$ amplitude, the effect of neglecting higher-order chiral terms is present in the large dependence of the amplitude on the meson mass, as well as in the neglect of final state interactions. One-loop chiral terms, if included, would bring the values for $\mathrm{Re}\,A_2$ down by approximately 30% or more (according to estimates in Ref. [19]).

Using results of Ref. [30] (accounting only chiral logs), we obtain that for the meson mass equal to kaon mass the ratio $\mathrm{Re}\,A_2/\mathrm{Re}\,A_0$ increases (i.e., $\Delta I=1/2$ rule becomes weaker) roughly by two times compared to the lowest order in chiral expansion.

Additional systematic errors are rather small compared to the chiral approximation error. The lattice cutoff dependence

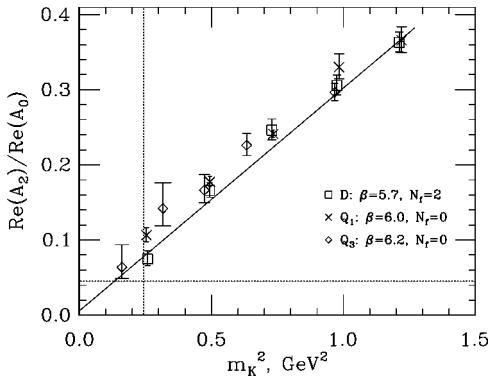

FIG. 13. $\mathrm{Re}\,A_2/\mathrm{Re}\,A_0$ vs the meson mass squared for quenched and dynamical ensembles. Ensembles Q_1 and D have comparable lattice spacings. Solid lines correspond to fits made through Q_1 and D data. The horizontal dashed line shows the experimental value of 1/22. The error bars show only the statistical errors obtained by JACKKNIFE.

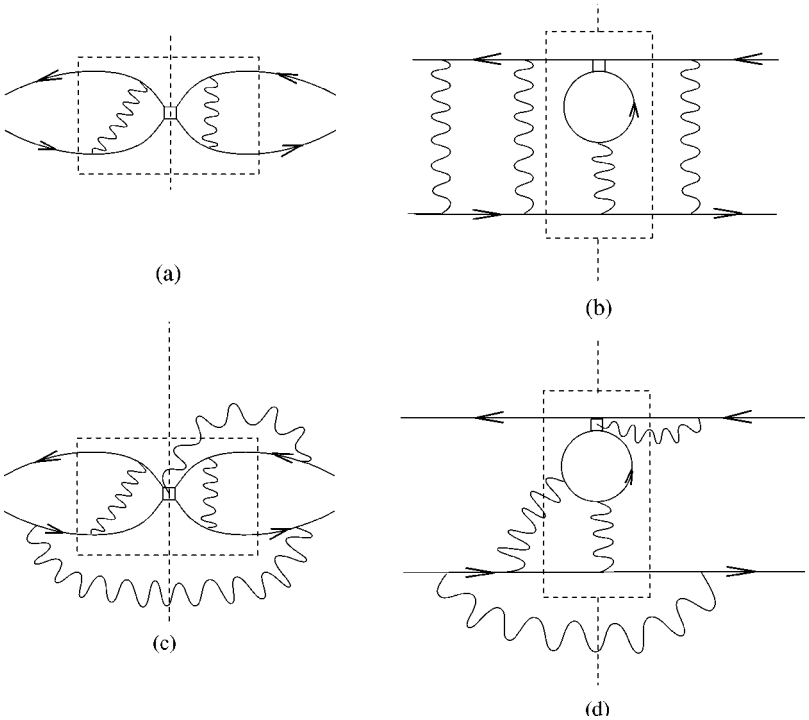

FIG. 14. Example of four kinds of diagrams with an arbitrary number of loops arising in renormalization of four-fermion operators: in (a) and (b) no propagator crosses the box or the axis; (c) and (d) exemplify the rest of the diagrams. The rectangle drawn in dotted line in (b) corresponds to operator structure PP_{EU}.

does not appear significant for this ratio, as opposed to each individual amplitude. Finite volume effects are smaller than noise. The error due to operator matching is estimated to be about 20% (see previous subsection and Sec. V A).

Keeping in mind the above systematic uncertainties, our results are broadly consistent with experiment. They confirm the understanding that most of the $\Delta I=1/2$ enhancement comes from the ''eye'' and ''annihilation'' diagrams.

V. OPERATOR MATCHING

As mentioned before, we have computed the matrix elements of all relevant operators with reasonable statistical accuracy. These are regulated in the lattice renormalization scheme. To get physical results, operators need to be matched to the same scheme in which the Wilson coefficients were computed in the continuum, namely $\overline{\text{MS}}$ NDR. While perturbative matching works quite well for $\text{Re}\,A_0$ and $\text{Re}\,A_2$, it seems to break down severely for matching operators relevant for ε'/ε.

A. Perturbative matching and $\text{Re}\,A_0$

Conventionally, lattice and continuum operators are matched using lattice perturbation theory:

$$O_i^{\text{cont}}(q^*)=O_i^{\text{lat}}+\frac{g^2(q^*a)}{16\pi^2}\sum_j\,(\gamma_{ij}\ln(q^*a)+C_{ij})O_j^{\text{lat}} +O(g^4)+O(a^n), \tag{27}$$

where γ_{ij} is the one-loop anomalous dimension matrix (the same in the continuum and on the lattice), and C_{ij} are finite coefficients calculated in one-loop lattice perturbation theory [31,32]. We use the ''horizontal matching'' procedure [33], whereby the same coupling constant as in the continuum ($g_{\overline{\text{MS}}}$) is used. The operators are matched at an intermediate scale q^* and evolved using the continuum renormalization group equations to the reference scale μ, which we take to be 2 GeV.

In calculation of $\text{Re}\,A_0$ and $\text{Re}\,A_2$, the main contributions come from left-left operators. One-loop renormalization factors for such (gauge-invariant) operators were computed by Ishizuka and Shizawa [31] (for current-current diagrams) and by Patel and Sharpe [32] (for penguin diagrams). These factors are fairly small, so at the first glance the perturbation theory seems to work well, in contrast with the case of left-right operators essential for estimating ε'/ε, as described below. However, even in the case of $\text{Re}\,A_0$ there is a certain ambiguity due to mixing of O_2 with O_6 through penguin diagrams. The matrix element of O_6 is rather large, so it

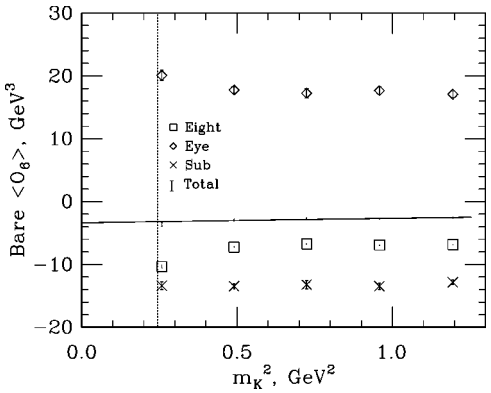

FIG. 15. Three contributions to $\langle\pi^+|O_6|K^+\rangle$: ''eight'' (boxes), ''eye'' (diamonds), and ''subtraction'' (crosses). These data represent bare operators for the dynamical ensemble. The fit is done for the sum total of all contributions.

TABLE VI. $\langle \pi^+\pi^-|O_6|K^0\rangle$ for the Q_1 ensemble in units of $(\mathrm{GeV})^3$ with tree-level matching (bare); with one-loop perturbative matching using two values of q^*; and with matching obtained by the partially nonperturbative procedure. The errors are statistical, except for the last line, where the first error is statistical, the second one comes from uncertainty in our determination of Z_S and Z_P, and the third one is an estimate of higher-order diagrams. As mentioned in the text, there is an unknown uncertainty in the partially nonperturbative procedure.

Quark mass	0.01	0.02	0.03	0.04	0.05
Bare	-2.95 ± 0.27	-2.61 ± 0.11	-2.50 ± 0.08	-2.60 ± 0.16	-2.94 ± 0.27
$q^*=\pi/a$	-0.69 ± 0.10	-0.66 ± 0.04	-0.66 ± 0.03	-0.73 ± 0.06	-0.83 ± 0.09
$q^*=1/a$	0.01 ± 0.07	-0.07 ± 0.03	-0.11 ± 0.02	-0.19 ± 0.04	-0.20 ± 0.03
Partially nonpert.	$2.03\pm0.07\pm0.42\pm0.62$	$0.74\pm0.03\pm0.37\pm0.02$	$0.44\pm0.02\pm0.31\pm0.03$	$0.23\pm0.03\pm0.28\pm0.02$	$0.25\pm0.05\pm0.36\pm0.02$

heavily influences $\langle O_2\rangle$ in spite of the small mixing coefficient. The operator O_6 receives enormous renormalization corrections in the first order, as discussed below. Therefore, there is an ambiguity as to whether the mixing should be evaluated with renormalized or bare O_6. That is, the higher-order diagrams [such as Figs. 14(b) and 14(d)] may be quite important here.

In order to estimate the uncertainty of neglecting higher-order diagrams, we evaluate the mixing with O_6 renormalized by the partially nonperturbative procedure described below, and compare it with results obtained by evaluating mixing with bare O_6. The first method amounts to resummation of those higher-order diagrams belonging only to type (b) in Fig. 14, while the second method ignores all higher-than-one-order corrections. Results quoted in the previous section were obtained by the first method, which is also close to using tree-level nondiagonal matching. The second method would produce values of $\mathrm{Re}\,A_0$ lower by about 20%. Thus we consider 20% a reasonable estimate of the matching uncertainty.

In calculating ε'/ε the operator matching issue becomes a much more serious obstacle as explained below.

B. Problems with perturbative matching

The value of ε'/ε depends on a number of subtle cancellations between matrix elements. In particular, in the existing literature O_6 and O_8 have been so far considered the most important operators whose contributions have opposite signs and almost cancel. Furthermore, the matrix elements of individual operators contain three main components (''eights,'' ''eyes,'' and ''subtractions''), which again conspire to almost cancel each other out (see Fig. 15). Thus ε'/ε is extremely sensitive to each of these components, and in particular to their matching.

Consider fermion contractions with operators such as

$$(PP)_{EU}=(\bar{s}\gamma_5\otimes\xi_5 u)(\bar{u}\gamma_5\otimes\xi_5 d), \tag{28a}$$

$$(SS)_{IU}=(\bar{s}\mathbb{1}\otimes\mathbb{1}d)(\bar{d}\mathbb{1}\otimes\mathbb{1}d), \tag{28b}$$

$$(PS)_{A2U}=(\bar{s}\gamma_5\otimes\xi_5 d)(\bar{d}\mathbb{1}\otimes\mathbb{1}d), \tag{28c}$$

which are main parts of, correspondingly, ''eight,'' ''eye,'' and ''subtraction'' components of O_6 and O_8 (see Appendix B). The finite renormalization coefficients for these operators have been computed in Ref. [32]. The diagonal coefficients are very large, so the corresponding one-loop corrections are in the neighborhood of -100% and strongly depend on which q^* is used (refer to Table VI). Thus perturbation theory fails in reliably matching the operators in Eqs. (28).

The finite coefficients for other (subdominant) operators, for example $(PP)_{EF}$, $(SS)_{EU}$, and $(SS)_{EF}$, are not known for formulation with gauge-invariant operators.[1] For illustration purposes, in Table VI we have used coefficients for gauge noninvariant operators computed in Ref. [32], but strictly speaking this is not justified.

To summarize, perturbative matching does not work and some of the coefficients are even poorly known. A solution would be to use a nonperturbative matching procedure, such as described in Ref. [34]. We have not completed this procedure. Nevertheless, can we say anything about ε'/ε at this moment?

C. Partially nonperturbative matching

As a temporary solution, we have adopted a partially nonperturbative operator matching procedure, which makes use of bilinear renormalization coefficients Z_P and Z_S. We compute the latter [35] following the nonperturbative method suggested by Martinelli *et al.* [36]. Namely we study the inverse of the ensemble-averaged quark propagator at large off-shell momenta in a fixed (Landau) gauge. An estimate of the renormalization of four-fermion operators can be obtained as follows.

Consider renormalization of the pseudoscalar-pseudoscalar operator in Eq. (28a). At the one-loop level, the diagonal renormalization coefficient C_{PP} (involving diagrams shown in Fig. 16) is almost equal to twice the pseu-

[1]Patel and Sharpe [32] have computed corrections for gauge-noninvariant operators. Operators in Eqs. (28) have zero distances, so the corrections are the same for gauge-invariant and the noninvariant operators. Renormalization of other operators (those having nonzero distances) generally differs from the gauge-noninvariant operators.

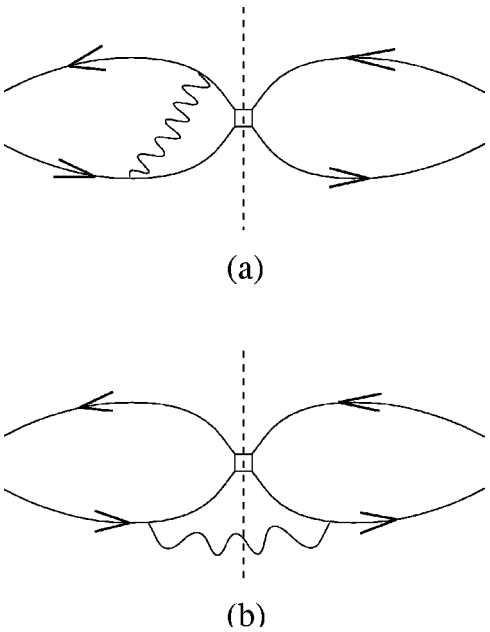

FIG. 16. Example of one-loop diagrams arising in renormalization of four-fermion operators: in type (a) no propagator crosses the axis, and type (b) includes the rest of the diagrams.

doscalar bilinear correction C_P. This suggests that, at least at one-loop level, the renormalization of $(PP)_{EU}$ comes mostly from diagrams in which no gluon propagator crosses the vertical axis of the diagram [for example, diagram (a) in Fig. 16], and very little from the rest of the diagrams [such as diagram (b) in Fig. 16]. In other words, the renormalization of $(PP)_{EU}$ would be identical to the renormalization of product of two pseudoscalar bilinears, were it not for the diagrams of type (b), which give a subdominant contribution. Mathematically,

$$(PP)^{\rm cont}_{EU}=(PP)^{\rm latt}_{EU}Z_{PP}+\cdots,$$

with

$$Z_{PP}=Z_P^2\left(1+\frac{g^2}{16\pi^2}\widetilde{C_{PP}}+O(g^4)\right), \tag{29}$$

$$Z_P=1+\frac{g^2}{16\pi^2}C_P+O(g^4), \tag{30}$$

and dots indicate mixing with other operators (nondiagonal part). The factor $\widetilde{C_{PP}}\equiv C_{PP}-2C_P$ contains diagrams of type (b) in Fig. 16 and is quite small.

In order to proceed, it may be reasonable to *assume* that the same holds at all orders in perturbation theory; namely the diagrams of type (c) in Fig. 14 give subdominant contribution compared to type (a) of the same figure. This assumption should be verified separately by performing nonperturbative renormalization procedure for four-fermion operators. If this ansatz is true, we can substitute the nonperturbative value of Z_P into Eq. (29) instead of using the perturbative expression from Eq. (30). Thus a partially nonperturbative estimate of $(PP)^{\rm cont}_U$ is obtained. This procedure is quite similar to the tadpole improvement idea: the bulk of diagonal renormalization is calculated nonperturbatively, while the rest is reliably computed in perturbation theory. Analogously we obtain diagonal renormalization of operators $(SS)_{IU}$ and $(PS)_{A2U}$ by using

$$Z_{SS}=Z_S^2\left(1+\frac{g^2}{16\pi^2}\widetilde{C_{SS}}+O(g^4)\right)$$

and

$$Z_{PS}=Z_SZ_P\left(1+\frac{g^2}{16\pi^2}\widetilde{C_{PS}}+O(g^4)\right).$$

(Note that $Z_P\neq Z_S$, even though they are equal in perturbation theory.) We match operators at the scale $q^*=1/a$ and use the continuum two-loop anomalous dimension to evolve to $\mu=2$ GeV.

Unfortunately, the above procedure does not completely solve the problem of operator renormalization, since it deals only with diagonal renormalization of the zero-distance operators in Eqs. (28). Even though these operators are dominant in contributing to ε'/ε, other operators [such as $(SS)_{EU}$ and $(PP)_{EF}$] can be important due to mixing with the dominant ones. The mixing coefficients for these operators are not known even in perturbation theory. For a reasonable estimate we use the coefficients obtained for gauge-noninvariant operator mixing [32].

Second, since renormalization of operators $(PP)_{EU}$, $(SS)_{IU}$, and $(PS)_{A2U}$ is dramatic,[2] their influence on other operators through nondiagonal mixing is ambiguous at one-loop order, even if the mixing coefficients are known. The ambiguity is due to higher-order diagrams (for example, those shown in Fig. 14). In order to partially resum them we use operators $(PP)_{EU}$, $(SS)_{IU}$, and $(PS)_{A2U}$ multiplied by factors Z_P^2, Z_S^2, and Z_PZ_S, correspondingly, whenever they appear in nondiagonal mixing with other operators. This is equivalent to evaluating the diagrams of type (a) and (b) in Fig. 14 at all orders, but ignoring the rest of the diagrams [such as diagrams (c) and (d) in Fig. 14] at all orders higher than first. A completely analogous procedure was used for mixing of O_6 with O_2 through penguins when evaluating $\mathrm{Re}\,A_0$. To estimate a possible error in this procedure we compare it with a simpler one, whereby bare operators are used in nondiagonal corrections (i.e., we apply strictly one-loop renormalization). The difference in ε'/ε between these two approaches is of the same order or even less than the error due to uncertainties in determination of Z_P and Z_S (see Tables VII and VIII).

[2]For example, at $m_q=0.01$ and $\mu=2$ GeV for the Q_1 ensemble we obtain $Z_{PP}=0.055\pm0.007$, $Z_{PS}=0.088\pm0.007$, and $Z_{SS}=0.142\pm0.010$.

TABLE VII. ε'/ε in units of 10^{-4} for Q_1 ensemble, computed in three ways: ($M1$) with $\mathrm{Re}\,A_0$ and $\mathrm{Re}\,A_2$ taken from experiment; ($M2$) with ω taken from experiment, and $\mathrm{Re}\,A_0$ amplitude from our simulation; ($M3$) with both $\mathrm{Re}\,A_0$ and $\mathrm{Re}\,A_2$ from our simulation. In all cases, partially nonperturbative matching has been used to obtain the results. In all perturbative corrections we have used one-loop nondiagonal coefficients computed for gauge-noninvariant operators, which are assumed to be of the same order as those for gauge-invariant operators. The first error is statistical (obtained by combining the individual errors in matrix elements by JACKKNIFE). The second error is the diagonal operator matching error due to uncertainty in the determination of Z_P and Z_S. In order to estimate the nondiagonal matching error we compare two renormalization procedures: using strictly one-loop nondiagonal corrections [denoted "(1-loop)"], and resumming part of higher-order corrections in nondiagonal mixing by using nonperturbative renormalization factors Z_P and Z_S (as explained in Sec. V C). The latter method is denoted "(p.r.)." Some other parameters used in obtaining these results are: $\mathrm{Im}\,\lambda_t = 1.5\times 10^{-4}$, $m_t = 170$ GeV, $m_b = 4.5$ GeV, $m_c = 1.3$ GeV, $\Omega_{\eta+\eta'} = 0.25$, $\alpha_{\overline{\mathrm{MS}}}^{(n_f=0)}(2\ \mathrm{GeV}) = 0.195$ (the latter is based on setting the lattice scale by ρ meson mass). Short distance coefficients were obtained by two-loop running using the anomalous dimension and threshold matrices computed by Buras *et al.* [15].

Quark mass	0.01	0.02	0.03	0.04	0.05
$M1$ (p.r.)	$-61.2\pm 2.8\pm 10.6$	$-27.4\pm 0.9\pm 8.9$	$-16.8\pm 0.5\pm 8.0$	$-8.0\pm 0.9\pm 7.2$	$-4.4\pm 0.9\pm 7.2$
$M1$ (1-loop)	$-52.3\pm 2.2\pm 10$	$-22.0\pm 0.8\pm 8.3$	$-12.2\pm 0.5\pm 6.9$	$-4.2\pm 1.1\pm 6.5$	$-1.2\pm 1.0\pm 6.6$
$M2$ (p.r.)	$-38.6\pm 2.1\pm 6.0$	$-18.7\pm 0.3\pm 7.0$	$-11.7\pm 0.2\pm 6.0$	$-6.1\pm 0.5\pm 5.3$	$-3.1\pm 0.5\pm 4.9$
$M2$ (1-loop)	$-45.4\pm 3.5\pm 8.6$	$-18.8\pm 0.4\pm 7.0$	$-10.3\pm 0.3\pm 6.0$	$-3.7\pm 0.8\pm 5.8$	$-0.9\pm 0.8\pm 5.2$
$M3$ (p.r.)	$-97\pm 14\pm 13$	$-81\pm 4\pm 23$	$-79\pm 2\pm 27$	$-81\pm 5\pm 38$	$-74\pm 4\pm 38$
$M3$ (1-loop)	$-142\pm 28\pm 29$	$-88\pm 5\pm 35$	$-75\pm 2\pm 39$	$-64\pm 4\pm 52$	$-55\pm 5\pm 51$

VI. ESTIMATES OF ε'/ε

Within the procedure outlined in Sec. V we have found that $\langle O_6\rangle$ has a different sign from the expected one due to a large renormalization factor. This translates into the negative sign of $\mathrm{Re}\,(\varepsilon'/\varepsilon)$ (Tables VII and VIII and Fig. 17).

Finite volume and quenching effects were found small compared to noise. Lattice cutoff dependence also seems to be small (see Fig. 18). The main uncertainty in estimating ε'/ε comes from operator matching, diagonal, and nondiagonal. For diagonal matching the uncertainty comes from: (1) statistical errors in the nonperturbative determination of Z_P and Z_S and from (2) unknown degree of validity of our ansatz in Sec. V C. For nondiagonal matching, the error is due to: (3) unknown nondiagonal coefficients in the mixing matrix and (4) ambiguity of accounting higher-order corrections. The error (1), as well as the statistical error, is quoted in Tables VII and VIII. The size of the error (4) can be judged by the spread in ε'/ε between two different approaches to higher-order corrections (strictly one-loop and partial resummation), also presented in Tables VII and VIII. The error (3) is likely to be of the same order as the error (4). The error (2) is uncontrolled at this point, since it is difficult to rigorously check our assumptions made in Sec. V C. In Fig. 17 we combine the statistical error with errors (1) and (4) in quadrature.

There are several ways to make a numerical prediction for ε'/ε. One can use the experimental values of $\mathrm{Re}\,A_0$ and $\mathrm{Re}\,A_2$ in Eq. (6) ($M1$), or one can use the values obtained on the lattice ($M3$). One can also adopt an intermediate strategy of using the experimental amplitude ratio ω and computed $\mathrm{Re}\,A_0$ ($M2$). All three methods are presented in Tables VII and VIII and Fig. 17. When the higher-order chiral corrections are taken into account and the continuum limit is taken (so that $\omega = 22$), these three methods should converge. In the meantime, the spread can be taken as an error estimator. In order to quote the central value we prefer the intermediate ($M2$) method, since herein the overall error due to final state interactions cancels between real and imaginary parts of A_0 amplitude, while the relative size of Π_0 and Π_2 contributions is given by the physical ω. Thereby we obtain

$$\mathrm{Re}(\varepsilon'/\varepsilon) = (-38.6\pm 2.1\ \ (\mathrm{stat})\pm 9.1\ \ (\mathrm{syst}))\times 10^{-4}. \tag{31}$$

The central value is based on quenched $\beta = 6.0$ data, taken at the kaon mass. The quoted systematic error includes only the errors (1) and (4) discussed above.

VII. CONCLUSIONS

We have presented in detail the setup of our calculation of hadronic matrix elements. Statistically reliable numbers for

TABLE VIII. ε'/ε results for the Q_3 ensemble ($\beta = 6.2$). See caption of Table VII for details.

Quark mass	0.005	0.010	0.015	0.020	0.030
$M1$ (p.r.)	$-68.1\pm 6.9\pm 36.0$	$-33.6\pm 2.9\pm 23.9$	$-24.9\pm 1.8\pm 22.0$	$-14.8\pm 1.0\pm 24.8$	$-10.3\pm 0.6\pm 19.6$
$M1$ (1-loop)	$-60.9\pm 6.9\pm 31.2$	$-29.3\pm 2.9\pm 21.0$	$21.4\pm 1.9\pm 19.4$	$-11.8\pm 1.1\pm 21.9$	$-7.9\pm 0.7\pm 17.3$
$M2$ (p.r.)	$-43.9\pm 9.5\pm 16.5$	$-33.1\pm 3.8\pm 18.3$	$-22.1\pm 1.2\pm 16.4$	$-14.2\pm 0.4\pm 20.3$	$-9.5\pm 0.3\pm 16.1$
$M2$ (1-loop)	$-53.6\pm 16.9\pm 25.0$	$-37.9\pm 6.0\pm 25.3$	$-23.0\pm 1.5\pm 20.0$	$-13.6\pm 0.6\pm 24.3$	$-8.5\pm 0.5\pm 18.0$
$M3$ (p.r.)	$-63.3\pm 35.1\pm 15.5$	$-103.9\pm 31.7\pm 45.2$	$-82.4\pm 12.9\pm 51.0$	$-74.9\pm 5.7\pm 88.0$	$-80.4\pm 3.9\pm 92.3$
$M3$ (1-loop)	$-98.3\pm 72.9\pm 46.2$	$-138.1\pm 53.1\pm 101.5$	$-92.4\pm 16.3\pm 86.3$	$-72.6\pm 5.7\pm 142.0$	$-73.5\pm 4.0\pm 131.0$

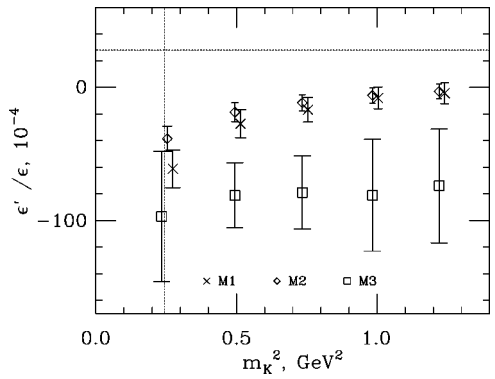

FIG. 17. An estimate of ε'/ε for the Q_1 ($\beta=6.0$) ensemble using the partially nonperturbative procedure described in the text. Three sets of points correspond to using experimental $\mathrm{Re}\,A_0$ and $\mathrm{Re}\,A_2$ in Eq. (6) (crosses), using our $\mathrm{Re}\,A_0$ but experimental ω (diamonds), or using $\mathrm{Re}\,A_0$ and $\mathrm{Re}\,A_2$ obtained from our calculations (squares). All other details are the same as in Table VII. The error shown is a combination of the statistical error, a matching error coming from uncertainties in the determination of Z_P and Z_S, and an estimated uncertainty in nondiagonal mixing of subdominant operators. The horizontal dashed line indicates the experimental value from Fermilab.

all operators in the basis defined in Eqs. (2) have been obtained. Based on these data we have made numerical estimates of $\mathrm{Re}\,A_0$, $\mathrm{Re}\,A_2$, and ε'/ε.

For the ratio of the $\Delta I=3/2$ and $\Delta I=1/2$ amplitudes we obtain

$$\frac{\mathrm{Re}\,A_2}{\mathrm{Re}\,A_0}=0.044\pm 0.010\ \ (\mathrm{stat})\pm 0.024\ \ (\mathrm{syst}). \qquad (32)$$

The central value is based on the dynamical $\beta=5.7$ estimate at $M=m_K/\sqrt{2}$. The systematic error includes mainly an estimated 50% uncertainty from higher-order chiral terms, including quenching effects. This estimation is based on a brief study of the effect of including the one-loop chiral logs (see Sec. IV C). Additional systematic errors are operator matching (estimated 20%), lattice cutoff dependence (less than noise), finite volume (less than noise).

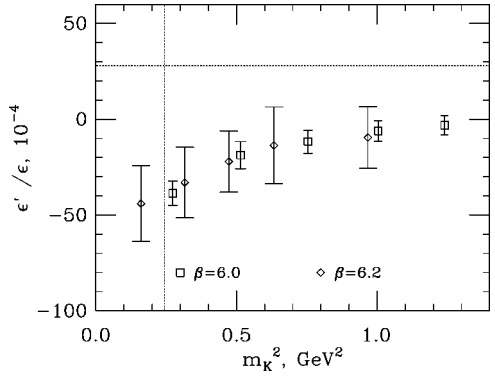

FIG. 18. A study of lattice cutoff dependence of $\mathrm{Re}\,(\varepsilon'/\varepsilon)$. Plotted data were obtained on $\beta=6.0$ and $\beta=6.2$ ensembles for the $M2$ method. The error bars show only the statistical error in matrix elements and in Z_S and Z_P constants. Systematic errors are significant but common to both ensembles. The horizontal dashed line indicates the experimental value from Fermilab.

To summarize, we find that $\Delta I=1/2$ transitions are enhanced with respect to $\Delta I=3/2$ ones (the ratio above is much less than 1), and that ''eye'' and ''annihilation'' diagrams are essential to such enhancement. The degree of enhancement, while estimated with sizable systematic error, is consistent with experiment.

As mentioned in the previous section, our numerical estimates of ε'/ε in Tables VII and VIII as well as Figs. 17 and 18 are also subject to considerable systematic uncertainties. As our ''best'' value, we quote

$$\mathrm{Re}(\varepsilon'/\varepsilon)=(-38.6\pm 2.1\ \ (\mathrm{stat})\pm 9.1\ \ (\mathrm{syst}))\times 10^{-4}. \qquad (33)$$

The central value is based on quenched $\beta=6.0$ data, taken at the kaon mass. The quoted systematic error includes the errors that can be estimated as discussed in Sec. VI. In addition, the following errors are not included (due to difficulty of estimation): (1) the validity of assumptions made in partial nonperturbative operator matching, and (2) higher-order chiral terms. The effects of quenching, finite volume, and finite lattice cutoff are found small compared to noise and other errors. In addition, our estimates of both ε'/ε and $\mathrm{Re}\,A_2/\mathrm{Re}\,A_0$ are subject to uncertainty due to the treatment of charm quark. This uncertainty includes higher-order QCD corrections and neglect of higher-dimensional charm quark operators, and is estimated to be on the order of 10%.

Due to the presence of potentially large systematic uncertainties in the above results, at present it is difficult to provide rigorous constraints on the standard model parameters. However, the negative sign of ε'/ε seems to be a stable feature in our numerical estimates and deserves some attention. Taken at face value, this result would contradict the experiment, which would mean that the minimal standard model does not describe direct CP violation adequately.

In order to decrease the above systematic errors a fully nonperturbative operator matching procedure should be performed and higher-order chiral terms should be calculated. These developments, together with the statistically significant values for $K\to\pi$ and $K\to 0$ matrix elements obtained in this work, can be used to achieve reliable numerical estimates both for the ε'/ε and $\Delta I=1/2$ rule in the future, thus providing more rigorous tests of the standard model.

ACKNOWLEDGMENTS

We acknowledge Lakshmi Venkataraman's help in developing supercomputer software. The Ohio Supercomputing Center and National Energy Research Scientific Computing Center (NERSC) have made this work possible by providing Cray-T3E computer time. We are grateful to the Columbia University group for access to their dynamical configurations.

APPENDIX A: EXPLICIT EXPRESSIONS FOR FERMION CONTRACTIONS

1. Quark operators

We work in the two flavor traces formalism when calculating contractions with four-fermion operators: for each contraction separately the operators are rendered in the form (if necessary, by Fierz transformation) of two bilinears with the flavor flow in the form of a product of two flavor traces. To be more precise, for ''eight'' contractions the operators are rendered in the form $(\bar{s}\Gamma u)(\bar{u}\Gamma d)$, while for the ''eye'' and ''annihilation'' contractions the appropriate form is $(\bar{s}\Gamma d)(\bar{q}\Gamma q)$. This is done in the continuum, before assigning the staggered fermion flavor.

The operator transcription in flavor space for staggered fermions is now standard [21], and we give it here for completeness. The Goldstone bosons have spin-flavor structure $\gamma_5 \otimes \xi_5$. The flavor structure of the operators is defined by requiring nonvanishing of the flavor traces, and so it depends on the contraction type: the flavor structure is ξ_5 in ''eights'' and two-point functions, $\mathbb{1}$ in ''eyes,'' and ''subtractions.'' In ''annihilation'' contractions the flavor structure is $\mathbb{1}$ for the bilinear in the quark loop trace and ξ_5 for the one involved in the external trace.

Either one or two color traces may be appropriate for a particular contraction with a given operator (see the next Appendix section for details). In one trace contractions (type ''*F*'' for ''fierzed'') the color flow is exchanged between the bilinears, while in two trace contractions (type ''*U*'' for ''unfierzed'') the color flow is contained within each bilinear so that the contraction is the product of two color traces. In either contraction type, when the distance between staggered fermion fields being color connected is nonzero, a gauge connector is inserted in the gauge-invariant fashion. The connector is computed as the average of products of gauge links along all shortest paths connecting the two sites. We also implement tadpole improvement by dividing each link in every gauge connector by $u_0 = [1/3\,\mathrm{Tr}(U_P)]^{1/4}$, where U_P is the average plaquette value.

2. Sources and contractions

We use local U(1) pseudofermion wall sources. Explicitly, we set up a field of U(1) phases $\xi_\alpha(\mathbf{x};t_0)$ ($|\xi|=1$) for each color and each site at a given timeslice t_0, which are chosen at random and satisfy

$$\langle \xi^*_\alpha(\mathbf{x};t_0)\, \xi_\beta(\mathbf{y};t_0)\rangle = \delta_{\alpha,\beta}\, \delta_{\mathbf{x},\mathbf{y}}. \tag{A1}$$

(Boldface characters designate spatial parts of the 4-vector with the same name.) We proceed to explain how this setup works in the case of the two-point function calculation, with trivial generalization to ''eight'' and ''annihilation'' contractions.

Consider the propagator from a wall at $t_0=0$ in a given background gauge configuration, computed by inverting the equation

$$(\not{D}+m)^{\alpha\beta}_{xy}\, \chi_\beta(y) = \xi_\alpha(\mathbf{x};0)\, \delta_{x_4,0}. \tag{A2}$$

This is equivalent to computing

$$\chi_\beta(y) = \sum_{\mathbf{x}}\ \xi_\alpha(\mathbf{x};0) G_{\beta\alpha}(y;\mathbf{x},0), \tag{A3}$$

where $G(y;x)$ is the propagator from four-point x to four-point y. For the staggered fermions description we label the fields by hypercube index h and the hypercube corner indices $A_\mu \in \{0,1\}^4$ instead of y. The two-point function is constructed as follows:

$$\mathrm{TP} \propto \sum_{h,A}\ \chi^*_\alpha(h,A) U_{\alpha\beta}(h,A,A+\Delta)\chi_\beta(h,A+\Delta) \times \phi(A)(-1)^A, \tag{A4}$$

where $\phi(A)$ and Δ_μ are phases and distances appropriate for a given staggered fermion operator,[3] $U(h,A,A+\Delta)$ is the appropriate gauge connector (see below), modulo 2 summation is implied for hypercube indices A, and h runs over all hypercubes in a given timeslice t where the operator is inserted. The factor $(-1)^A$ takes into account that for staggered fermions $G(x;y) = G^\dagger(y;x)(-1)^x(-1)^y$. Equation (A4) corresponds to

$$\mathrm{TP} \propto \sum_{\mathbf{x},\mathbf{y},\mathbf{z}}\ G_{\alpha\beta}(z,y)\Gamma G_{\beta\gamma}(y,x)(-1)^z \xi^*_\alpha(z)\xi_\gamma(x), \tag{A5}$$

where Γ is used for simplicity to show the appropriate operator structure. The summation over $\mathbf{x}$ and $\mathbf{z}$ over the entire spatial volume averages over the noise, so the last equation is equivalent to

$$\mathrm{TP} \propto \sum_{\mathbf{x},\mathbf{y}}\ \mathrm{tr}\, G(x,y)\, \Gamma\, G(y,x)(-1)^x. \tag{A6}$$

Therefore, using the pseudofermion wall source is equivalent to summation of contractions obtained with independent local delta-function sources. Note that the factor $(-1)^x$ and zero distance in the staggered fermions language are equivalent to spin-flavor structure $\gamma_5 \otimes \xi_5$. This means the source creates pseudoscalar mesons at rest, which includes Goldstone bosons. Strictly speaking, this source also creates mesons with spin-flavor structure $\gamma_5\gamma_4 \otimes \xi_5\xi_4$, since it is defined only on one timeslice. However, as explained in the first footnote in Sec. 2.3 of Ref. [21], these states do not contribute.

We have used one copy of pseudofermion sources per configuration. Analogously, we construct the pion sink at

[3] For a given bilinear with spin-flavor structure $\Gamma_S \otimes \Gamma_F$, these are determined as follows: $\Delta_\mu = |S_\mu - F_\mu|^2$ and $\phi(A) = \frac{1}{4}\mathrm{Tr}(\Gamma_A^\dagger \Gamma_S \Gamma_{A+\Delta} \Gamma_F^\dagger)$, where S_μ and F_μ are spin and flavor vectors such that $\Gamma_S = \gamma_1^{S_1}\gamma_2^{S_2}\gamma_3^{S_3}\gamma_4^{S_4}$ and $\Gamma_F = \gamma_1^{F_1}\gamma_2^{F_2}\gamma_3^{F_3}\gamma_4^{F_4}$, and $\Gamma_A = \gamma_1^{A_1}\gamma_2^{A_2}\gamma_3^{A_3}\gamma_4^{A_4}$.

time T by using another set of U(1) random noise ($\langle \xi^*_\alpha(\mathbf{x};T)\xi_\beta(\mathbf{y};T)\rangle = \delta_{\alpha,\beta}\delta_{\mathbf{x},\mathbf{y}}$, $|\xi|=1$). The propagator Φ is computed as follows:

$$(\not{D}+m)^{\alpha\beta}_{xy}\Phi_\beta(y)=\xi_\alpha(\mathbf{x};T)\delta_{x_4,T}. \tag{A7}$$

Suppose Δ_1, $\Delta_2\in\{0,1\}^4$ and $\phi_1(A)$, $\phi_2(A)$ are distances and phases of the two staggered fermion bilinears making up a given four-fermion operator. The expression for the "eight" contraction [Fig. 1(a)] with two color traces ("U" type) is given by

$$\begin{aligned}E_U\propto\sum_{h,A,B}&\chi^*_\alpha(h,A)U_{\alpha\beta}(h,A,A+\Delta_1)\chi_\beta(h,A+\Delta_1)\\&\times\phi_1(A)(-1)^A\Phi^*_\rho(h,B)U_{\rho\sigma}(h,B,B+\Delta_2)\\&\times\Phi_\sigma(h,B+\Delta_2)\phi_2(B)(-1)^B,\end{aligned} \tag{A8}$$

up to various normalization factors which cancel in the B ratio. In this expression A, $B\in\{0,1\}^4$ run over 16 hypercube corners (modulo 2 summation is implied for these indices). The hypercube index h, as before, runs over the entire spatial volume of the timeslice t of the operator insertion. The gauge connector $U(h,A,B)$ is the identity matrix when $A=B$, otherwise it is the average of products of gauge links in the given configuration along all shortest paths from A to B in a given hypercube h. The expression Eq. (A8), as well as all other contractions, is computed for each background gauge configuration and is subject to averaging over the configurations. (Whenever several contractions are combined in a single quantity, such as a B ratio, we use JACKKNIFE to estimate the statistical error.)

The expression for one color trace ("F" type) contraction is similar:

$$\begin{aligned}E_F\propto\sum_{h,A,B}&\chi^*_\alpha(h,A)U_{\alpha\beta}(h,A,B+\Delta_2)\chi_\sigma(h,A+\Delta_1)\\&\times\phi_1(A)(-1)^A\Phi^*_\rho(h,B)U_{\rho\sigma}(h,B,A+\Delta_1)\\&\times\Phi_\beta(h,B+\Delta_2)\phi_2(B)(-1)^B.\end{aligned} \tag{A9}$$

For "eye" and "subtraction" diagrams [Figs. 1(b) and 1(d)] the source setup is a little more involved, since the kaon and pion are directly connected by a propagator. In order to construct a wall source we need to compute the product

$$\psi(y)=\sum_{\mathbf{x}} G(\mathbf{y},t;\mathbf{x},T)\cdot G(\mathbf{x},T;\mathbf{0},0)(-1)^x.$$

In order to avoid computing propagators from every point $\mathbf{x}$ at the timeslice T, we first compute propagator $G(\mathbf{x},T;\mathbf{0},0)$, cut out the timeslice T, and use it as the source for calculating the propagator to $(\mathbf{y},t)$. This amounts to inverting the equation

$$(\not{D}+m)^{\alpha\beta}_{xy}\psi_\beta(y)=\chi_\alpha(x)\delta_{(x_4,T)}(-1)^x, \tag{A10}$$

where $\chi_\alpha(x)$ is the propagator from the wall source at $t_0=0$ defined in Eq. (A2). We use the following expression for evaluating the "subtraction" diagram:

$$S\propto\sum_{h,A}\chi^*_\alpha(h,A)U_{\alpha\beta}(h,A,A+\Delta)\psi_\beta(h,A+\Delta)\phi(A)(-1)^A. \tag{A11}$$

Again, averaging over the noise leaves only local connections in both sources, so in the continuum language we get

$$S\propto\sum_{\mathbf{x},\mathbf{y},\mathbf{z}}\mathrm{tr}\,G(\mathbf{x},0;\mathbf{z},t)\Gamma G(\mathbf{z},t;\mathbf{y},T)G(\mathbf{y},T;\mathbf{x},0)(-1)^x(-1)^y. \tag{A12}$$

[In fact, we are mostly interested in subtracting the operator $\overline{s}\mathbb{1}\otimes\mathbb{1}d$, so in Eq. (A11) $\Delta=0,0,0,0$ and $\phi(A)=1$.]

In order to efficiently compute fermion loops for "eye" and "annihilation" diagrams [Figs. 1(b) and 1(c)], we use U(1) noise copies $\zeta^{(i)}$, $i=1,\ldots,N$, at every point in spacetime. We compute $\eta^{(i)}$ by inverting $(\not{D}+m)\eta^{(i)}=\zeta^{(i)}$. It is easy to convince oneself that the propagator from y to x equals

$$G(x;y)=\langle\eta_x\zeta^*_y\rangle. \tag{A13}$$

In practice we average over $N=10$ noise copies. This includes two or four copies of the lattice in time extension, so the real number of noise copies is 20 or 40, with another factor of 3 for color. The efficiency of this method is crucial for obtaining good statistical precision.

The expressions for "U" and "F" type "eye" diagrams are as follows:

$$\begin{aligned}I_U\propto\sum_{h,A,B}&\chi^*_\alpha(h,A)U_{\alpha\beta}(h,A,A+\Delta_1)\psi_\beta(h,A+\Delta_1)\\&\times\phi_1(A)(-1)^A\frac{1}{N}\sum_{i=1}^N\zeta^{(i)}_\rho{}^*(h,B)U_{\rho\sigma}(h,B,B+\Delta_2)\\&\times\eta^{(i)}_\sigma(h,B+\Delta_2)\phi_2(B)(-1)^B,\end{aligned} \tag{A14}$$

$$\begin{aligned}I_F\propto\sum_{h,A,B}&\chi^*_\alpha(h,A)U_{\alpha\sigma}(h,A,B+\Delta_2)\psi_\beta(h,A+\Delta_1)\\&\times\phi_1(A)(-1)^A\frac{1}{N}\sum_{i=1}^N\zeta^{(i)}_\rho{}^*(h,B)U_{\rho\beta}(h,B,A+\Delta_1)\\&\times\eta^{(i)}_\sigma(h,B+\Delta_2)\phi_2(B)(-1)^B.\end{aligned} \tag{A15}$$

The computation of "annihilation" diagrams [Fig. 1(c)] is similar to the two-point function, except the fermion loop is added and the derivative with respect to the quark mass difference m_d-m_s is inserted in turn in every strange quark propagator. Derivatives of the propagators are given by inverting equations

$$(\not{D}+m)\chi'=\chi, \tag{A16}$$

$$(\not{D}+m)\eta'^{(i)}=\eta^{(i)}. \tag{A17}$$

We have, therefore, four kinds of ''annihilation'' contractions, which should be combined in an appropriate way for each operator depending on the quark flavor structure (this is spelled out in Appendix B):

$$A_{1U}\propto\sum_{h,A,B}\chi'^{*}_{\alpha}(h,A)U_{\alpha\beta}(h,A,A+\Delta_1)\chi_{\beta}(h,A+\Delta_1)\times\phi_1(A)(-1)^A\frac{1}{N}\sum_{i=1}^{N}\zeta^{(i)*}_{\rho}(h,B)U_{\rho\sigma}(h,B,B+\Delta_2)\times\eta^{(i)}_{\sigma}(h,B+\Delta_2)\phi_2(B)(-1)^B, \tag{A18}$$

$$A_{1F}\propto\sum_{h,A,B}\chi'^{*}_{\alpha}(h,A)U_{\alpha\sigma}(h,A,B+\Delta_2)\chi_{\beta}(h,A+\Delta_1)\times\phi_1(A)(-1)^A\frac{1}{N}\sum_{i=1}^{N}\zeta^{(i)*}_{\rho}(h,B)U_{\rho\beta}(h,B,A+\Delta_1)\times\eta^{(i)}_{\sigma}(h,B+\Delta_2)\phi_2(B)(-1)^B, \tag{A19}$$

$$A_{2U}\propto\sum_{h,A,B}\chi^{*}_{\alpha}(h,A)U_{\alpha\beta}(h,A,A+\Delta_1)\chi_{\beta}(h,A+\Delta_1)\times\phi_1(A)(-1)^A\frac{1}{N}\sum_{i=1}^{N}\zeta^{(i)*}_{\rho}(h,B)U_{\rho\sigma}(h,B,B+\Delta_2)\times\eta'^{(i)}_{\sigma}(h,B+\Delta_2)\phi_2(B)(-1)^B, \tag{A20}$$

$$A_{2F}\propto\sum_{h,A,B}\chi^{*}_{\alpha}(h,A)U_{\alpha\sigma}(h,A,B+\Delta_2)\chi_{\beta}(h,A+\Delta_1)\times\phi_1(A)(-1)^A\frac{1}{N}\sum_{i=1}^{N}\zeta^{(i)*}_{\rho}(h,B)U_{\rho\beta}(h,B,A+\Delta_1)\times\eta'^{(i)}_{\sigma}(h,B+\Delta_2)\phi_2(B)(-1)^B. \tag{A21}$$

APPENDIX B: EXPLICIT EXPRESSIONS FOR MATRIX ELEMENTS IN TERMS OF FERMION CONTRACTIONS

Operators in Eqs. (2) can be decomposed into $I=0$ and $I=2$ parts, which contribute, correspondingly, to $\Delta I=1/2$ and $\Delta I=3/2$ transitions. Here we give the expressions for these parts for completeness, since $\mathrm{Re}\,A_0$, $\mathrm{Re}\,A_2$, and ε'/ε are directly expressible in terms of their matrix elements. The $I=0$ parts are given as follows:

$$O_1^{(0)}=\tfrac{2}{3}(\bar{s}\gamma_\mu(1-\gamma_5)d)(\bar{u}\gamma^\mu(1-\gamma_5)u)-\tfrac{1}{3}(\bar{s}\gamma_\mu(1-\gamma_5)u)\times(\bar{u}\gamma^\mu(1-\gamma_5)d)+\tfrac{1}{3}(\bar{s}\gamma_\mu(1-\gamma_5)d)\times(\bar{d}\gamma^\mu(1-\gamma_5)d), \tag{B1}$$

$$O_2^{(0)}=\tfrac{2}{3}(\bar{s}\gamma_\mu(1-\gamma_5)u)(\bar{u}\gamma^\mu(1-\gamma_5)d)-\tfrac{1}{3}(\bar{s}\gamma_\mu(1-\gamma_5)d)\times(\bar{u}\gamma^\mu(1-\gamma_5)u)+\tfrac{1}{3}(\bar{s}\gamma_\mu(1-\gamma_5)d)\times(d\gamma^\mu(1-\gamma_5)d), \tag{B2}$$

$$O_3^{(0)}=(\bar{s}\gamma_\mu(1-\gamma_5)d)\sum_{q=u,d,s}(\bar{q}\gamma^\mu(1-\gamma_5)q), \tag{B3}$$

$$O_4^{(0)}=(\bar{s}_\alpha\gamma_\mu(1-\gamma_5)d_\beta)\sum_{q=u,d,s}(\bar{q}_\beta\gamma^\mu(1-\gamma_5)q_\alpha), \tag{B4}$$

$$O_5^{(0)}=(\bar{s}\gamma_\mu(1-\gamma_5)d)\sum_{q=u,d,s}(\bar{q}\gamma^\mu(1+\gamma_5)q), \tag{B5}$$

$$O_6^{(0)}=(\bar{s}_\alpha\gamma_\mu(1-\gamma_5)d_\beta)\sum_{q=u,d,s}(\bar{q}_\beta\gamma^\mu(1+\gamma_5)q_\alpha), \tag{B6}$$

$$O_7^{(0)}=\tfrac{1}{2}[(\bar{s}\gamma_\mu(1-\gamma_5)d)(\bar{u}\gamma^\mu(1+\gamma_5)u)-(\bar{s}\gamma_\mu(1-\gamma_5)u)(\bar{u}\gamma^\mu(1+\gamma_5)d)-(\bar{s}\gamma_\mu(1-\gamma_5)d)\times(\bar{s}\gamma^\mu(1+\gamma_5)s)], \tag{B7}$$

$$O_8^{(0)}=\tfrac{1}{2}[(\bar{s}_\alpha\gamma_\mu(1-\gamma_5)d_\beta)(\bar{u}_\beta\gamma^\mu(1+\gamma_5)u_\alpha)-(\bar{s}_\alpha\gamma_\mu(1-\gamma_5)u_\beta)(\bar{u}_\beta\gamma^\mu(1+\gamma_5)d_\alpha)-(\bar{s}_\alpha\gamma_\mu(1-\gamma_5)d_\beta)(\bar{s}_\beta\gamma^\mu(1+\gamma_5)s_\alpha)], \tag{B8}$$

$$O_9^{(0)}=\tfrac{1}{2}[(\bar{s}\gamma_\mu(1-\gamma_5)d)(\bar{u}\gamma^\mu(1-\gamma_5)u)-(\bar{s}\gamma_\mu(1-\gamma_5)u)(\bar{u}\gamma^\mu(1-\gamma_5)d)-(\bar{s}\gamma_\mu(1-\gamma_5)d)(\bar{s}\gamma^\mu(1-\gamma_5)s)], \tag{B9}$$

$$O_{10}^{(0)}=\tfrac{1}{2}[(\bar{s}\gamma_\mu(1-\gamma_5)u)(\bar{u}\gamma^\mu(1-\gamma_5)d)-(\bar{s}\gamma_\mu(1-\gamma_5)d)(\bar{u}\gamma^\mu(1-\gamma_5)u)-(s\gamma_\mu(1-\gamma_5)d)(s\gamma^\mu(1-\gamma_5)s)]. \tag{B10}$$

Expressions for the $I=2$ parts are as follows:

$$O_1^{(2)}=O_2^{(2)}=\tfrac{2}{3}O_9^{(2)}=\tfrac{2}{3}O_{10}^{(2)}=\tfrac{1}{3}[(\bar{s}\gamma_\mu(1-\gamma_5)u)(\bar{u}\gamma^\mu(1-\gamma_5)d)+(\bar{s}\gamma_\mu(1-\gamma_5)d)(\bar{u}\gamma^\mu(1-\gamma_5)u)-(\bar{s}\gamma_\mu(1-\gamma_5)d)(\bar{d}\gamma^\mu(1-\gamma_5)d)], \tag{B11}$$

$$O_7^{(2)}=\tfrac{1}{2}[(\bar{s}\gamma_\mu(1-\gamma_5)u)(\bar{u}\gamma^\mu(1+\gamma_5)d)+(\bar{s}\gamma_\mu(1-\gamma_5)d)(\bar{u}\gamma^\mu(1+\gamma_5)u)-(\bar{s}\gamma_\mu(1-\gamma_5)d)(\bar{d}\gamma^\mu(1+\gamma_5)d)] \tag{B12}$$

$$O_8^{(2)}=\tfrac{1}{2}[(\bar{s}_\alpha\gamma_\mu(1-\gamma_5)u_\beta)(\bar{u}_\beta\gamma^\mu(1+\gamma_5)d_\alpha)+(\bar{s}_\alpha\gamma_\mu(1-\gamma_5)d_\beta)(\bar{u}_\beta\gamma^\mu(1+\gamma_5)u_\alpha)-(\bar{s}_\alpha\gamma_\mu(1-\gamma_5)d_\beta)(\bar{d}_\beta\gamma^\mu(1+\gamma_5)d_\alpha)] \tag{B13}$$

$$O_3^{(2)}=O_4^{(2)}=O_5^{(2)}=O_6^{(2)}=0. \tag{B14}$$

(Whenever the color indices are not shown, they are contracted within each bilinear, i.e., there are two color traces.)

As mentioned in Sec. III B, in order to compute matrix elements of $I=0$ operators one needs to evaluate three types of diagrams: ''eight'' [Fig. 1(a)], ''eye'' [Fig. 1(b)], and ''annihilation'' [Fig. 1(c)]. In Appendix A we have given detailed expressions for computation of these contractions, given the spin-flavor structure. Here we assign this structure to all contractions required for each operator, i.e., we express each matrix element in terms of contractions which were ''built'' in the previous section.

Let us introduce some notation. The matrix element of the above operators has three components:

$$\langle \pi^+\pi^-|O_i|K^0\rangle = (E_i + I_i - S(2m\alpha_i))\frac{m_K^2 - m_\pi^2}{(p_\pi \cdot p_K)f}, \tag{B15}$$

where m is the common quark mass for s, d, and u, and

$$\alpha_i = \frac{A_i}{P}. \tag{B16}$$

Here E_i and I_i stand for ''eight'' and ''eye'' contractions of the $\langle \pi^+|O_i|K^+\rangle$ matrix element, $A_i \sim \langle 0|O_i|K^0\rangle/(m_d - m_s)$ is the ''annihilation'' diagram, $S=\langle \pi^+|\bar{s}d|K^+\rangle$ is the ''subtraction'' diagram, and $P=\langle 0|\bar{s}\gamma_5 d|K^0\rangle$ is the two-point function. We compute α_i by averaging the ratio on the right-hand side of Eq. (B16) over a suitable time range.

Detailed expressions for E_i, I_i, and A_i are given below in terms of the basic contractions on the lattice. We label basic contractions by two letters, each representing a bilinear. For example, PP stands for contraction of the operator with spin structure $(\gamma_5)(\gamma_5)$, SS is for $(\mathbb{1})(\mathbb{1})$, VV stands for $(\gamma_\mu)(\gamma^\mu)$, and AA is for $(\gamma_\mu\gamma_5)(\gamma^\mu\gamma_5)$. The staggered flavor is determined by the type of contraction, as explained in Appendix A. Basic contractions are also labeled by their subscript. The first letter indicates whether it is an ''eight,'' ''eye,'' or ''annihilation'' contraction, and the second is ''U'' for two, or ''F'' for one color trace. For example, PP_{EU} stands for the ''eight'' contraction of the operator with spin-flavor structure $(\gamma_5\otimes\xi_5)(\gamma_5\otimes\xi_5)$ with two color traces; VA_{A1F} stands for the ''annihilation'' contraction of the first type, in which the derivative is taken with respect to quark mass on the external leg (see Appendix A), the spin-flavor structure is $(\gamma_\mu\otimes\xi_5)(\gamma^\mu\gamma_5\otimes\mathbb{1})$, and one color trace is taken. What follows are the full expressions.[4]

''Eight'' parts:

$$E_1^{(0)} = \tfrac{2}{3}(VV_{EF}+AA_{EF}) - \tfrac{1}{3}(VV_{EU}+AA_{EU}), \tag{B17}$$

$$E_2^{(0)} = \tfrac{2}{3}(VV_{EU}+AA_{EU}) - \tfrac{1}{3}(VV_{EF}+AA_{EF}), \tag{B18}$$

$$E_3^{(0)} = VV_{EF}+AA_{EF}, \tag{B19}$$

$$E_4^{(0)} = VV_{EU}+AA_{EU}, \tag{B20}$$

$$E_5^{(0)} = 2(PP_{EF}-SS_{EF}), \tag{B21}$$

$$E_6^{(0)} = 2(PP_{EU}-SS_{EU}), \tag{B22}$$

$$E_7^{(0)} = SS_{EF} - PP_{EF} + \tfrac{1}{2}(VV_{EU}-AA_{EU}), \tag{B23}$$

$$E_8^{(0)} = SS_{EU} - PP_{EU} + \tfrac{1}{2}(VV_{EF}-AA_{EF}), \tag{B24}$$

$$E_9^{(0)} = -E_{10}^{(0)} = \tfrac{1}{2}(VV_{EF}+AA_{EF}-VV_{EU}-AA_{EU}), \tag{B25}$$

$$E_1^{(2)} = E_2^{(2)} = \tfrac{2}{3}E_9^{(2)} = \tfrac{2}{3}E_{10}^{(2)} = \tfrac{1}{3}(VV_{EU}+AA_{EU}+VV_{EF}+AA_{EF}), \tag{B26}$$

$$E_3^{(2)} = E_4^{(2)} = E_5^{(2)} = E_6^{(2)} = 0, \tag{B27}$$

$$E_7^{(2)} = \tfrac{1}{2}(AA_{EU}-VV_{EU}) + SS_{EF} - PP_{EF}, \tag{B28}$$

$$E_8^{(2)} = \tfrac{1}{2}(AA_{EF}-VV_{EF}) + SS_{EU} - PP_{EU}. \tag{B29}$$

''Eye'' parts:

$$I_1^{(0)} = VV_{IU}+AA_{IU}, \tag{B30}$$

$$I_2^{(0)} = VV_{IF}+AA_{IF}, \tag{B31}$$

$$I_3^{(0)} = 3(VV_{IU}+AA_{IU}) + 2(VV_{IF}+AA_{IF}), \tag{B32}$$

$$I_4^{(0)} = 3(VV_{IF}+AA_{IF}) + 2(VV_{IU}+AA_{IU}), \tag{B33}$$

$$I_5^{(0)} = 3(VV_{IU}-AA_{IU}) + 4(PP_{IF}-SS_{IF}), \tag{B34}$$

$$I_6^{(0)} = 3(VV_{IF}-AA_{IF}) + 4(PP_{IU}-SS_{IU}), \tag{B35}$$

$$I_7^{(0)} = 2(PP_{IF}-SS_{IF}), \tag{B36}$$

$$I_8^{(0)} = 2(PP_{IU}-SS_{IU}), \tag{B37}$$

$$I_9^{(0)} = VV_{IF}+AA_{IF}, \tag{B38}$$

$$I_{10}^{(0)} = VV_{IU}+AA_{IU}. \tag{B39}$$

''Annihilation'' parts are obtained by inserting the derivative with respect to $(m_d - m_s)$ into every propagator involving the strange quark:

$$A_1^{(0)} = -(VA_{A1U}+AV_{A1U}), \tag{B40}$$

$$A_2^{(0)} = -(VA_{A1F}+AV_{A1F}), \tag{B41}$$

$$A_3^{(0)} = -3(VA_{A1U}+AV_{A1U}) - (VA_{A2U}+AV_{A2U}) - 2(VA_{A1F}+AV_{A1F}) - (VA_{A2F}+AV_{A2F}), \tag{B42}$$

$$A_4^{(0)} = -3(VA_{A1F}+AV_{A1F}) - (VA_{A2F}+AV_{A2F}) - 2(VA_{A1U}+AV_{A1U}) - (VA_{A2U}+AV_{A2U}), \tag{B43}$$

[4]Signs of operators O_7 and O_8 have been changed in order to be consistent with the sign convention of Buras *et al.* [3].

$$A_5^{(0)} = 3(VA_{A1U} - AV_{A1U}) + (VA_{A2U} - AV_{A2U}) + 2(PS_{A2F} - SP_{A2F}), \quad \text{(B44)}$$

$$A_6^{(0)} = 3(VA_{A1F} - AV_{A1F}) + (VA_{A2F} - AV_{A2F}) + 2(PS_{A2U} - SP_{A2U}), \quad \text{(B45)}$$

$$A_7^{(0)} = \tfrac{1}{2}(VA_{A2U} - AV_{A2U}) + (PS_{A2F} - SP_{A2F}), \quad \text{(B46)}$$

$$A_8^{(0)} = \tfrac{1}{2}(VA_{A2F} - AV_{A2F}) + (PS_{A2U} - SP_{A2U}), \quad \text{(B47)}$$

$$A_9^{(0)} = VA_{A1F} + AV_{A1F} + \tfrac{1}{2}(VA_{A2U} + AV_{A2U} + VA_{A2F} + AV_{A2F}), \quad \text{(B48)}$$

$$A_{10}^{(0)} = VA_{A1U} + AV_{A1U} + \tfrac{1}{2}(VA_{A2F} + AV_{A2F} + VA_{A2U} + AV_{A2U}). \quad \text{(B49)}$$

Of course, ''eye'' and ''annihilation'' contractions are not present in $I=2$ operators.

[1] KTeV Collaboration, A. Alavi-Harati *et al.*, Phys. Rev. Lett. **83**, 22 (1999).
[2] NA48 Collaboration, V. Fanti *et al.*, Phys. Lett. B **465**, 335 (1999).
[3] A. Buras *et al.*, Nucl. Phys. **B408**, 209 (1993); A. Buras, hep-ph/9806471; in *Probing the Standard Model of Particle Interactions*, edited by F. David and R. Gupta (Elsevier, Amsterdam, 1998); S. Bosch *et al.*, Nucl. Phys. **B565**, 3 (2000).
[4] G. Kilcup, Nucl. Phys. B (Proc. Suppl.) **20**, 417 (1991); S. Sharpe, *ibid.* **20**, 429 (1991); S. Sharpe *et al.*, Phys. Lett. B **192**, 149 (1987).
[5] C. Bernard, T. Draper, G. Hockney, and A. Soni, Nucl. Phys. B (Proc. Suppl.) **4**, 483 (1988).
[6] C. Bernard and A. Soni, Nucl. Phys. B (Proc. Suppl.) **17**, 495 (1990).
[7] C. Bernard and A. Soni, Nucl. Phys. B (Proc. Suppl.) **9**, 155 (1989).
[8] M.B. Gavela *et al.*, Nucl. Phys. B (Proc. Suppl.) **7A**, 228 (1989); Phys. Lett. B **211**, 139 (1988); E. Franco *et al.*, Nucl. Phys. B (Proc. Suppl.) **4**, 466 (1988).
[9] G. Martinelli *et al.*, Nucl. Phys. B (Proc. Suppl.) **17**, 523 (1990).
[10] C. Bernard, in *From Actions To Answers*, Proceedings of TASI, Boulder, Colorado, 1989, edited by T. DeGrand and D. Toussaint (World Scientific, Singapore, 1990).
[11] JLQCD Collaboration, S. Aoki *et al.*, Phys. Rev. D **58**, 054503 (1998).
[12] L. Lellouch, Nucl. Phys. B (Proc. Suppl.) **94**, 142 (2001).
[13] T. Blum, Nucl. Phys. B (Proc. Suppl.) **94**, 291 (2001).
[14] CP-PACS Collaboration, A. Ali Khan *et al.*, Nucl. Phys. B (Proc. Suppl.) **94**, 287 (2001).
[15] R. Mawhinney, Nucl. Phys. B (Proc. Suppl.) **94**, 315 (2001).
[16] M. Ciuchini *et al.*, Z. Phys. C **68**, 239 (1995).
[17] L. Maiani and M. Testa, Phys. Lett. B **245**, 585 (1990).
[18] C. Bernard, T. Draper, A. Soni, H.D. Politzer, and M.B. Wise, Phys. Rev. D **32**, 2343 (1985).
[19] M. Golterman and K.C. Leung, Phys. Rev. D **56**, 2950 (1997).
[20] G. Kilcup and S. Sharpe, Nucl. Phys. **B283**, 493 (1987).
[21] S. Sharpe *et al.*, Nucl. Phys. **B286**, 253 (1987).
[22] F.R. Brown *et al.*, Phys. Rev. Lett. **67**, 1062 (1991).
[23] G. Kilcup and D. Pekurovsky, Nucl. Phys. B (Proc. Suppl.) **53**, 345 (1997).
[24] S. Gottlieb, Nucl. Phys. B (Proc. Suppl.) **53**, 155 (1997).
[25] D. Chen and R. Mawhinney, Nucl. Phys. B (Proc. Suppl.) **53**, 216 (1997).
[26] J.F. Donoghue, E. Golowich, and B.R. Holstein, Phys. Lett. **119B**, 412 (1982).
[27] JLQCD Collaboration, S. Aoki *et al.*, Phys. Rev. Lett. **80**, 5271 (1998).
[28] S. Sharpe, Phys. Rev. D **46**, 3146 (1992).
[29] J. Kambor *et al.*, Phys. Lett. B **261**, 496 (1991).
[30] M. Golterman and E. Pallante, Nucl. Phys. B (Proc. Suppl.) **83**, 250 (2000).
[31] N. Ishizuka and Y. Shizawa, Phys. Rev. D **49**, 3519 (1994).
[32] S. Sharpe and A. Patel, Nucl. Phys. **B417**, 307 (1994).
[33] R. Gupta, T. Bhattacharya, and S. Sharpe, Phys. Rev. D **55**, 4036 (1997).
[34] A. Donini *et al.*, Nucl. Phys. B (Proc. Suppl.) **53**, 883 (1997); A. Donini *et al.*, Phys. Lett. B **360**, 83 (1995).
[35] D. Pekurovsky and G. Kilcup (unpublished).
[36] G. Martinelli, C. Pittori, C.T. Sachrajda, M. Testa, and A. Vladikas, Nucl. Phys. **B445**, 81 (1995).